Inorganic Chemistry
Cite This: Inorg. Chem. 2018, 57, 3371−3386
Article
pubs.acs.org/IC

Substituted versus Naked Thiourea Ligand Containing Pseudotetrahedral Cobalt(II) Complexes: A Comparative Study on Its Magnetization Relaxation Dynamics Phenomenon

Shefali Vaidya,[†] Pragya Shukla,[†] Shalini Tripathi,[†] Eric Rivière,[‡] Talal Mallah,*[,‡] Gopalan Rajaraman,*[,†] and Maheswaran Shanmugam*[,†]

[†]Department of Chemistry, Indian Institute of Technology (IIT) Bombay, Powai, Mumbai, 400076 Maharashtra, India
[‡]Institut de Chimie Moléculaire et des Matériaux d'Orsay, CNRS, Université Paris Sud and Université Paris Saclay, Orsay, Cedex 91405, France

Supporting Information

ABSTRACT: A series of mononuclear tetrahedral cobalt(II) complexes with the general molecular formula $[Co(L_1)_2X_2]$ [where L_1 = tetramethylthiourea ($[(CH_3)_2N]_2C{=}S$) and X = Cl (**1**), Br (**2**), and I (**3**)] were isolated, and their structures were characterized by single-crystal X-ray diffraction. The experimental direct-current magnetic data are excellently reproduced by fitting both $\chi_M T(T)$ and $M(H)$ simultaneously using the spin Hamiltonian (SH) parameters $D_1 = -18.1$ cm^{-1} and $g_{1,iso} = 2.26$, $D_2 = -16.4$ cm^{-1} and $g_{2,iso} = 2.33$, and $D_3 = -22$ cm^{-1} and $g_{3,iso} = 2.4$ for **1**−**3**, respectively, and the sign of D was unambiguously confirmed from X-band electron paramagnetic resonance measurements. The effective energy barrier extracted for the magnetically diluted complexes **1**−**3** (10%) is larger than the barrier observed for the pure samples and implies a nonzero contribution of dipolar interaction to the magnetization relaxation dynamics. The SH parameters extracted for the three complexes drastically differ from their respective parent complexes that possess the general molecular formula $[Co(L)_2X_2]$ [where L = thiourea ($[(NH_2)_2C{=}S]$ and X = Cl (**1a**), Br (**2a**), and I (**3a**)], which is rationalized by detailed ab initio calculations. An exhaustive theoretical study reveals that both the ground and excited states are not pure but rather multideterminental in nature (**1**−**3**). Noticeably, the substitution of L by L_1 induces structural distortion in **1**−**3** on the level of the secondary coordination sphere compared to **1a**−**3a**. This distortion leads to an overall reduction in $|E/D|$ of **1**−**3** compared to **1a**−**3a**. This may be one of the reasons for the origin of the slower relaxation times of **1**−**3** compared to **1a**−**3a**.

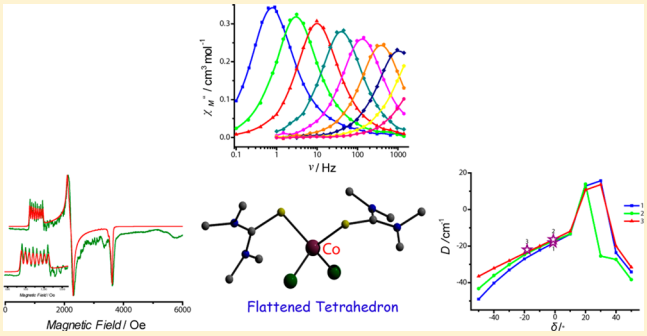

INTRODUCTION

Single-molecule magnets (SMMs) are a class of discrete molecules that show superparamagnetic behavior below a certain blocking temperature (T_B)[1−4] and are of purely molecular origin. This phenomenon is predominantly governed by the occurrence of Ising-type magnetic anisotropy resulting from the simultaneous effects of structural distortion and spin−orbit coupling, acting on a spin state S, known as zero-field splitting (zfs). The energy barrier to the reorientation of the magnetization is thus, within this model, equal to DS^2 (for integer S values), where D is the axial ZFS parameter. Because D is proportional to $1/S^2$,[5] attempts to increase the energy barrier by increasing the ground-state spin value S of transition-metal-containing polynuclear complexes turned out not to be a successful strategy, but the investigation of such systems was valuable for understanding the different processes that govern the relaxation time and the experimentally measured effective energy barriers (U_{eff}).[6−12] Because of the persistent problem associated with larger oligomeric clusters ($D \propto 1/S^2$), researchers turned their focus to single-ion magnets (SIMs). In SIMs, however, the ground state of the molecule is fixed and the only parameter available to control U_{eff} is D. Orbital angular momentum is the dominant factor that dictates the magnitude of D, and the orbital angular momentum is regulated by the coordination number (geometry) and oxidation state of the (first-row transition-)metal ion. So, by altering the geometry around the metal ions, one can fine-tune the electronic structure of the metal ions.[13−34] This scenario has been witnessed in several mononuclear complexes where ligand-field-controlled spin−orbit coupling facilitates the magnetization blockade.[13−19,35−37] In particular, the classical approach (by reducing the coordination number) employed to gain a large orbital angular momentum by Long and co-workers in a two-coordinate iron(I) complex and other linear complexes of cobalt(II) by Gao and co-workers results in a record-high anisotropic barrier.[35,37]

Received: January 18, 2018
Published: February 27, 2018

DOI: 10.1021/acs.inorgchem.8b00160
Inorg. Chem. 2018, 57, 3371−3386

Apart from the classical approach, efforts have been taken to fine-tune the spin Hamiltonian (SH) parameters of various metal ions by some other means. For example, simply replacing the lighter halide with heavier halides in certain chromium(III) octahedral complexes brought a change in the magnitude of D.[38] Similarly, varying the strength of the ligand field in certain iron(II) complexes appears to be a promising approach.[19] Even more intricate parameters, such as changing the substituent on the aromatic ligand coordinated to the cobalt(II) ion, have an influence on the electronic structure of the metal ion, as reported by Powell and co-workers.[39] The in-plane and out-of-plane positions of the cobalt(II) ion in a square-pyramidal geometry were found to be another alternate pathway to tune the anisotropic barrier.[40] Of late, Dunbar and co-workers reported a rare and promising trigonal-antiprism geometry shown by cobalt(II) complexes that adds further understanding about the origin of slow relaxation of magnetization and the mechanism involved in these complexes.[41] Various nickel(II) complexes in certain enforced geometries stabilize large D (200 cm^{-1}), and the rationale for stabilizing such a huge D value has been detailed by Mallah and co-workers and Murrie and co-workers elsewhere independently.[21,33,42] Because of the under-barrier tunneling mechanisms in integer spin systems, slow relaxation of magnetization is absent even in the presence of an external magnetic field. Nevertheless, such problems encountered in integer spin systems can be overcome using metal ions containing noninteger spin values to design the SIMs[16−18,24,27,28,43−45] Presumably, this is ultimately the reason behind numerous reports based on cobalt(II) complexes in various geometries, particularly pseudotetrahedral geometry, in the literature compared to other metal ions.[17,18,20,30,32,34,36,46]

Several parameters potentially can be employed to rationally stabilize easy-axis or Ising-type magnetic anisotropy in tetrahedral cobalt(II) complexes, which is exemplified by various research groups including us. The metal−ligand covalence is observed to be the predominant factor in controlling the D value in T_d cobalt(II) ions, which recently was elegantly explained by Long and co-workers and us.[20,30,32,36] Variation in the counter cation also seems to have a drastic effect on alteration of the sign of magnetic anisotropy from negative to positive.[23] Although several methodologies are proposed in the literature to switch the sign and fine tune the magnitude and tune the magnitude of anisotropy, control of the SH parameters by ligand design is still scarce in the literature.[20,30−32,36,47] In addition, we did show that, by increasing the number of soft donors around the tetrahedral cobalt(II) ion, the D value can be increased, which was rationalized by detailed computational calculations.[23,29,32,36] The influence of the other commonly used ligands like halides (chlorine, bromine, and iodine) to fine-tune the D value of cobalt(II) complexes with the general formula $[Co(L)_2(X_2)]$ [where L = thiourea and X = Cl (**1a**), Br (**2a**), and I (**3a**)], in addition to the role of a soft donor, was investigated by us recently.[34]

In a natural extension of this work, we probe the role of the substituent on the ligand and its influence in determining the sign and magnitude of D and its relaxation dynamics. In this article, we report a series of pseudotetrahedral cobalt(II) complexes with the molecular formula $[Co(L_1)_2(X_2)]$ [where L_1 = tetramethylthiourea ($[(CH_3)_2N]_2C{=}S$) and X = Cl (**1**), Br (**2**), and I (**3**)], which are structurally characterized by single-crystal X-ray diffraction. We have investigated their (**1**−**3**) detailed direct-current (dc) and alternating-current (ac) relaxation phenomena. Drastic changes were observed in magnetization relaxation dynamics in complexes **1**−**3**, which were rationalized with the help of ab initio CASSCF calculations. The substituent on the thiourea ligand (second coordination sphere) appears to have a non-negligible influence on the magnitude of D.

EXPERIMENTAL SECTION

All reactions were carried out under aerobic conditions unless otherwise mentioned. All of the chemicals and solvents utilized were purchased from commercially available sources (Alfa Aesar or Sigma Aldrich) and used without any further purification. The magnetic data were collected on a MPMS-XL SQUID magnetometer equipped with a 70 kOe magnet in the temperature range of 2−300 K. Single-crystal X-ray diffraction for complexes **1**−**3** was performed on a Rigaku Saturn CCD diffractometer using a graphite monochromator (λ = 0.71073 Å). The unit cell determination and data reduction were performed using *CrysAlisPro 1.171.38.43* (Rigaku OD, 2015). With the help of *SHELXL-2014/7*[48] (Sheldrick, 2014), the structures were solved by direct methods and refined by least-squares procedures on F^2. All non-hydrogen atoms were refined anisotropically, and hydrogen atoms were refined as riding models (CCDC 1817777−1817779 for complexes **1**−**3**, respectively). X-band electron paramagnetic resonance (EPR) spectra were recorded using a Bruker EMXPLUS spectrometer, and the EPR spectra were simulated using *EasySpin* software (version 5.2.11).[49] All of the quantum-chemical calculations performed on the X-ray structures of complexes **1**−**3** were done using the *ORCA* suite.[50] Multireference ab initio calculations were used to calculate the SH parameters. State-average complete-active-space self-consistent-field (CASSCF)[51] calculations were performed on all of the complexes along with the NEVPT2 module, as implemented in the *ORCA* suite. The ZORA[52,53] method was used for the treatment of scalar relativistic effects. The Ahlrichs polarized triple-ζ (TZVP)[54,55] quality basis set, along with TZV/J auxiliary basis sets for the resolution of identity (RI) approximation, was used for all of the atoms. The calculations were performed with an active space of CAS(7,5), which corresponds to seven active d electrons in five active d orbitals and computed 10 quartet as well as 40 doublet states in the CI procedure to extract the desired SH parameters.

EXPERIMENTAL PROCEDURES

Synthesis of $[Co(L_1)_2Cl_2]$ [1, Where L_1 = Tetramethylthiourea ($[(CH_3)_2N]_2C{=}S$)]. L_1 (1 g, 7.5 mmol) was added to a warm (35−40 °C) ethanolic solution of $CoCl_2{\cdot}6H_2O$ (0.897 g, 3.8 mmol). The reaction mixture was heated under reflux for 12 h and then allowed to cool to room temperature (RT) before the solvent is removed under reduced pressure. Blue block-shaped crystals of **1**, suitable for X-ray diffraction, were grown in 1 day from an ethyl acetate filtrate upon slow evaporation. Yield (based on $CoCl_2{\cdot}6H_2O$): 0.87 g (58.3%). Calcd: C, 30.46; H, 6.13; N, 14.21; S, 16.26. Found: C, 31.02; H, 6.11; N, 14.6; S, 16.19. IR (KBr, cm^{-1}): 3320, 3401 (ν_{NH_2}), 1643 ($\nu_{C=S}$).

Synthesis of Complex $[Co(L_1)_2X_2]$, Where X = Br (2) and I (3). A synthetic procedure similar to that of **1** was followed for the isolation of **2** or **3**, but in place of $CoCl_2{\cdot}6H_2O$, $CoBr_2$ (0.825 g, 3.8 mmol) or CoI2 (1.19 g, 3.8 mmol) was used. Yield for **2** (based on $CoBr_2$): 1.1 g (60%). Calcd: C, 24.86; H, 5.01; N, 11.60; S, 13.27. Found: C, 24.52; H, 4.97; N, 11.51; S, 13.19. IR (KBr, cm^{-1}): 3325, 3382 (ν_{NH_2}), 1647 ($\nu_{C=S}$). Yield for **3** (based on CoI_2): 1.6 g (73.1%). Calcd: C, 20.81; H, 4.19; N, 9.71; S, 11.11. Found: C, 20.65; H, 4.37; N, 9.56; S, 11.45. IR (KBr, cm^{-1}): 3318, 3422 (ν_{NH_2}), 1652 ($\nu_{C=S}$).

The polycrystalline phase purity of all of the complexes (**1**−**3**) was confirmed by powder X-ray diffraction (PXRD). The PXRD profile of all of the complexes (**1**−**3**) is in excellent agreement with the simulated data, which was derived from its corresponding single-crystal X-ray data (Figure S1).

Synthesis of $[Zn(L_1)_2X_2]$, Where X = Cl (4), Br (5), and I (6). The same synthetic procedure as that for **1** was employed for the isolation of complexes **4**−**6**, but the corresponding ZnX_2 [X = Cl

DOI: 10.1021/acs.inorgchem.8b00160
Inorg. Chem. 2018, 57, 3371−3386

(0.516 g, 3.8 mmol), Br (0.852 g, 3.8 mmol), or I (1.2 g, 3.8 mmol)] was used instead of $CoCl_2·6H_2O$. Colorless block-shaped crystals of **4**–**6**, suitable for X-ray diffraction were grown from an ethyl acetate filtrate upon slow evaporation in 1 day. Yield for **4** (based on $ZnCl_2$): 1.02 g (67.1%). Calcd: C, 29.97; H, 6.04; N, 13.98; S, 16.00. Found: C, 29.81; H, 6.3; N, 13.56; S, 16.05. IR (KBr, cm^{-1}): 3355, 3382 (ν_{NH_2}), 1598 ($\nu_{C=S}$). Yield for **5** (based on $ZnBr_2$): 1.08 g (58.4%). Calcd: C, 24.53; H, 4.94; N, 11.44; S, 13.10. Found: C, 24.72; H, 5.13; N, 11.58; S, 13.32. IR (KBr, cm^{-1}): 3294, 3452 (ν_{NH_2}), 1633 ($\nu_{C=S}$). Yield for **6** (based on ZnI_2): 1.46 g (66.7%). Calcd: C, 20.58; H, 4.14; N, 9.6; S, 10.99. Found: C, 20.81; H, 4.34; N, 9.4; S, 10.69. IR (KBr, cm^{-1}): 3356, 3412 (ν_{NH_2}), 1614 ($\nu_{C=S}$).

The unit cells of complexes **4**–**6** were checked and found to be in excellent agreement with their respective paramagnetic cobalt(II) analogues. This indicates that the diamagnetic zinc(II) complexes (**4**–**6**) are isomorphous to **1**–**3**, i.e., the same space group and packing diagram as their paramagnetic analogues. This is further corroborated by the PXRD profiles. The experimental PXRD patterns of **4**–**6** are in good agreement with the simulated data of the corresponding paramagnetic analogues **1**–**3** (Figure S2).

Synthesis of 10% Diluted Samples of 1. $CoCl_2·6H_2O$ (0.09 g, 0.38 mmol) and $ZnCl_2$ (0.463 g, 3.4 mmol) in solid form were added to warm ethanol (35–40 °C). When the metal salts were completely dissolved, L_1 (1 g, 7.5 mmol) was added to the solution, and the reaction mixture was heated under reflux for 12 h. The reaction mixture was allowed to cool to RT. The solvent was removed by rotovap, resulting in sky-blue crude materials. Pale-blue block-shaped crystals of 10% diluted samples of **1** were grown from an ethyl acetate filtrate within 24 h upon slow evaporation.

Synthesis of 10% Diluted Samples of 2 and 3. A similar synthetic procedure was followed to isolate single crystals of 10% magnetically diluted **2** and **3**, but corresponding ZnX_2 [X = Br (0.768 g, 3.4 mmol) or I (1.09 g, 3.4 mmol)] was used in place of $ZnCl_2$.

RESULTS AND DISCUSSION

The reaction of various cobalt dihalide salts with symmetrically substituted ligand L_1 in an alcoholic solution led to the isolation of blue/green single crystals (Scheme 1) of the targeted complexes upon crystallization in ethyl acetate.

Scheme 1. General Synthetic Procedure Followed To Isolate Complexes 1–3

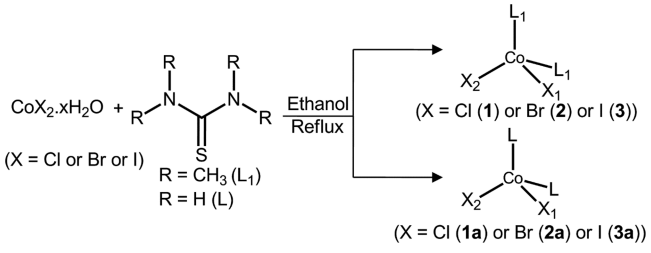

Single-crystal X-ray diffraction measurements reveal that the molecular formula of these complexes is $[CoX_2(L_1)_2]$, where X = Cl (**1**), Br (**2**), and I (**3**) (Figure 1). All three complexes crystallize in the monoclinic space groups $P2_1/n$ (for **1** and **2**) and $C2/c$ (for **3**) (Table S1).

X-ray studies clearly show that all three complexes are mononuclear and have similar molecular structures. The divalent cobalt(II) ion in each complex (**1**–**3**) is surrounded by two neutral L_1 ligands, and the charge balance is brought by two halide ligands (chloride, bromide, and iodide for **1**–**3**, respectively; Figure 1). The average Co–S bond length was found to be almost same for the three complexes: equal to 2.344(9), 2.345(9), and 2.338(9) Å for **1**–**3**, respectively.

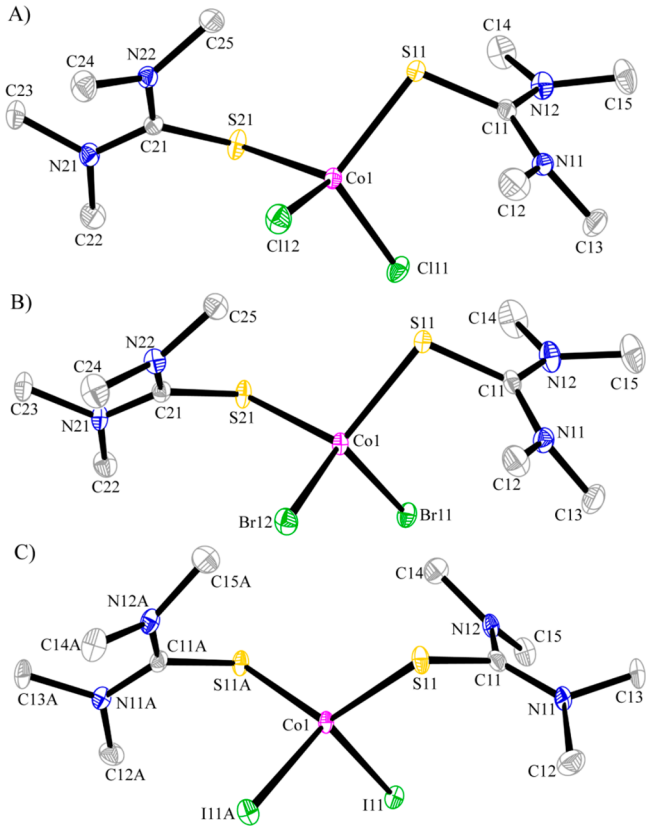

Figure 1. Thermal ellipsoid (50% probability) representations of the crystal structures of complexes **1**–**3** in parts A–C, respectively.

In contrast, there is a significant increase in the average cobalt–halide bond lengths [Co–Cl = 2.255(10) Å for **1**; Co–Br = 2 0.402(6) Å for **2**; Co-I = 2.600(3) Å for **3**] due to the increase in the size of the ligand as we move down group 17. The observed bond lengths in these complexes are consistent with the other tetrahedral cobalt(II) complexes reported in the literature.[47,56] Unlike the trend observed in the cobalt–halide bond length, there is no large deviation in the X–Co–X angles [$\angle$X11–Co^{II}–X12 of 114.11° (for **1**), 113.53° (for **2**), and 112.08° (for **3**)], while considerable change in the S–Co–S angles is noticed; in particular, the deviation is much larger for **3** ($\angle$S11–Co^{II}–S12 = 125.19°) than for **1** or **2** [$\angle$S11–Co^{II}–S12 = 106.18° (for **1**) and 106.59° (for **2**)]. The X-ray structural parameters show that the four-coordinate cobalt(II) ions have a distorted tetrahedral geometry. The extent of deviation from the ideal tetrahedral geometry was qualitatively confirmed by employing continuous-shape measurement software.[57]

From Table S1, it is very well witnessed that complexes **1** and **2** possess almost the same crystallographic parameters; hence, these complexes have similar packing arrangements, while complex **3** shows distinct packing diagrams compared to **1** or **2** because of its drastic change in the unit cell parameters. A representative packing diagram for **1** and **3** is shown in Figure 2 (see also Figure S3). The packing diagrams of all three complexes (**1**–**3**) were analyzed carefully, which revealed that the closest $Co^{II}\cdots Co^{II}$ distances were found to be 7.909(2), 8.340(8), and 8.737(5) Å, respectively. All three complexes show both intermolecular and intramolecular hydrogen bonding between the $-CH_3$ group and halides or sulfur within the crystal lattice. The relative strength of hydrogen bonding in

DOI: 10.1021/acs.inorgchem.8b00160
Inorg. Chem. 2018, 57, 3371–3386

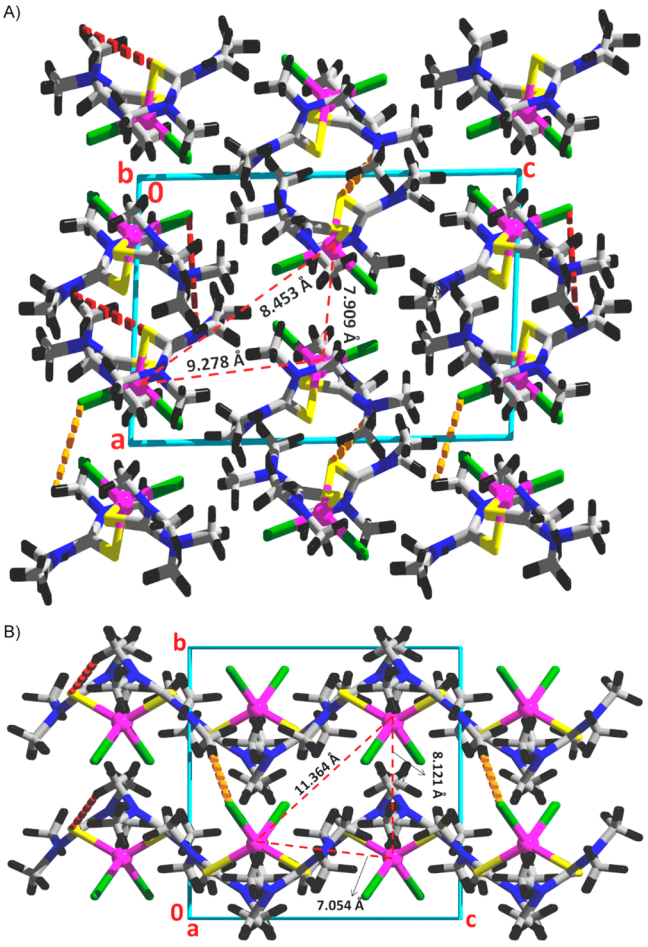

Figure 2. Packing diagrams of complexes **1** (panel A) and **3** (panel B). Orange dotted lines represent intermolecular hydrogen bonding, and red dotted lines represent intramolecular hydrogen bonding.

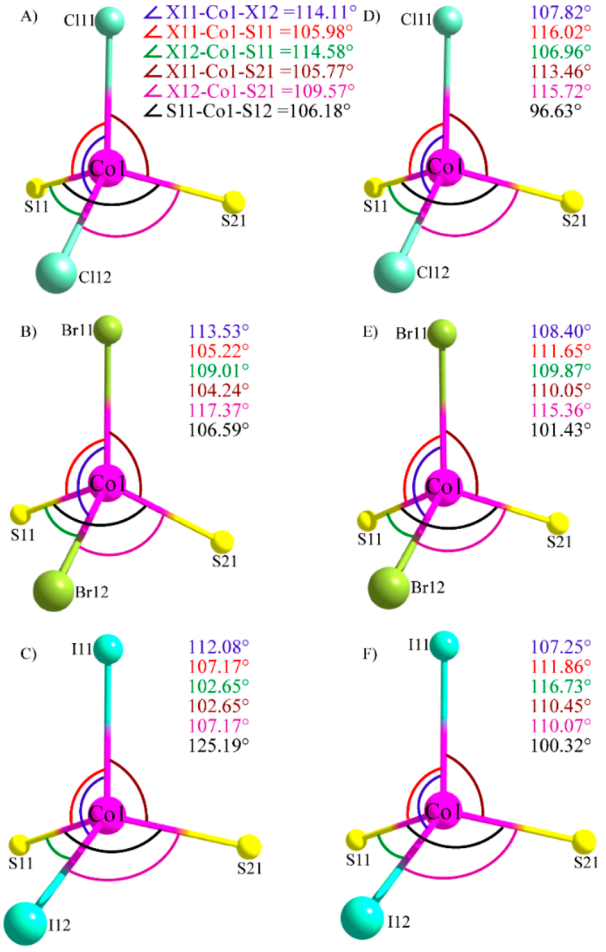

Figure 3. Influence of substitution on the structural parameters in **1**−**3** (panels A−C, respectively) compared with their parent analogues **1a**−**3a** (panels D−F, respectively).

1 or **2** is quite strong compared to **3**; this could be correlated with the $Co^{II}\cdots Co^{II}$ distance found within the crystal lattice. The presence of an extended supramolecular network is likely to have a significant influence on the relaxation dynamics of these complexes (vide infra). The atoms involved in both intra- and intermolecular hydrogen bonding are compiled in Table S2.

Effect of Substitution on the Structural Parameters of 1−3 with Their Parent Complexes 1a−3a. As mentioned earlier, the objective of this report is to investigate the effect of the second coordination sphere of the cobalt(II) ions, brought about by substituting the thiourea ligand (L)[34] by tetramethylthiourea (L_1) on the magnetic properties of complexes **1**−**3**. To better understand the magnetic properties of these complexes, we have analyzed the crystal structures of both **1**−**3** and their parent analogues **1a**−**3a** (Figures 3 and S4).

The following major changes were noticed in the structural parameters when comparing the **1**−**3** series to their **1a**−**3a** analogues (Figure 3): (1) there is a slight increase in the observed Co−S bond distances (from 0.02 to 0.04 Å) in **1**−**3** compared to **1a**−**3a**, (2) there is no considerable change in Co−X distances (Figure S4), (3) there is a drastic increase in the X−Co−X and S−Co−S [∠X−Co−X (5−6° increase) and ∠S−Co−S (5−25° increase)] angles observed for **1**−**3** compared to **1a**−**3a** (Figure 3), and (4) finally, because of substitution on the parent thiourea ligand, the observed shortest Co···Co distance is increased in **1**−**3** compared to **1a**−**3a** [Co···Co = 6.12 Å (**1a**), 5.85 Å (**2a**), and 5.93 Å (**3a**)], which results in weak supramolecular hydrogen-bonding networks in **1**−**3** compared to **1a**−**3a**. Overall, it can be concluded that substitution on the thiourea ligand induces significant distortion in the coordination sphere of cobalt(II), which may have a significant influence on the magnetic anisotropy and, consequently, on the relaxation of magnetization of the complexes (vide infra).

dc Magnetic Susceptibility Measurement of 1−3. The temperature-dependent magnetic susceptibility measurements on polycrystalline samples of **1**−**3** were carried out between 2 and 300 K in the presence of a static external magnetic field of 1 kOe. The RT $\chi_M T$ values of **1**−**3** are 2.58, 2.72, and 2.82 cm^3 K mol^{-1}, respectively (Figure 4). The experimentally observed RT $\chi_M T$ values are slightly higher than the expected one (1.875 cm^3 K mol^{-1}) of a high-spin cobalt(II) paramagnetic complex with no first-order orbital angular momentum and an average g value of 2.0. The relatively large $\chi_M T$ values observed are presumably due to the ligand-field-induced structural distortion, resulting in a second-order orbital angular momentum contribution to the total magnetic moment of the complexes. When the temperature is lowered, $\chi_M T$ linearly decreases from RT to ~40 K, which could be attributed to the combined effects of $S = {}^3/_2$ sublevel depopulation and/or temperature-independent paramagnetism (TIP) that is accounted for when

DOI: 10.1021/acs.inorgchem.8b00160
Inorg. Chem. 2018, 57, 3371−3386

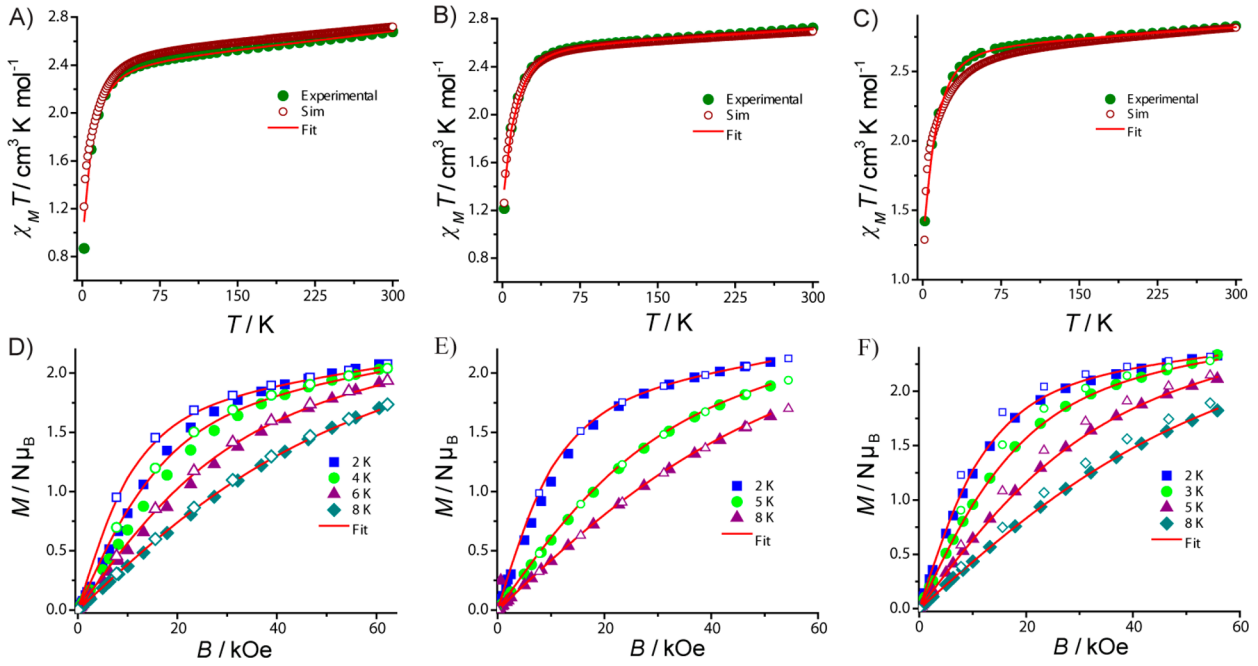

Figure 4. (A–C) Temperature-dependent dc magnetic susceptibility measurement performed on the polycrystalline samples of **1**–**3**, respectively, in the presence of a 1 kOe magnetic field. (D–F) Field-dependent magnetization measurements performed at the indicated temperatures for complexes **1**–**3**. The solid red lines in all of the panels represent the best fits obtained for the experimental magnetic data using the parameters described in the main text [simultaneous fitting of the magnetic data of both $\chi_M T(T)$ and $M(B)$ using *PHI*]. Open symbols in all of the panels represent simulations of the experimental magnetic data using the computed SH parameters. Note: Here **g** tensors obtained from the experimental fits and D and E/D from NEVPT2 are employed for the simulation of data. Because only a smaller reference space is employed in these calculations, the g factors are generally overestimated because the metal–ligand covalancy is not fully addressed.

fitting the data (see below). Below 40 K, $\chi_M T$ drops drastically to the final values of 0.8, 1.2, and 1.3 cm^3 K mol^{-1} at 2 K for **1**–**3**, respectively (Figure 4). The drop of $\chi_M T$ below 40 K is due to the magnetic anisotropy (zfs), which lifts the degeneracy of the $S = {}^3/_2$ sublevels.

Field-dependent magnetization measurements were performed for **1**–**3** at 2, 3, 5, and 8 K. The data have the shape expected for mononuclear cobalt(II) complexes with relatively large magnetic anisotropy, where saturation is not reached at the highest magnetic field available (70 kOe; Figures 4 and S5).[33,56] In order to extract the SH parameters of complexes **1**–**3**, the experimental magnetic data of both $\chi_M T(T)$ and $M(B)$ were fitted simultaneously using the *PHI* software[58] by employing the Hamiltonian

$$\mathcal{H} = \beta \mathbf{S}\cdot\bar{\bar{\mathbf{g}}}\cdot\mathbf{B} + D\left[S_z^2 - \frac{1}{3}S(S+1)\right] + E(S_x^2 - S_y^2) \quad (1)$$

where $\bar{\bar{\mathbf{g}}}$ is the g matrix, β is the bohr magneton, **B** is the external magnetic field, **S** is the spin operator, S is the spin value, and D and E are the axial and rhombic anisotropy parameters, respectively. To avoid overparametrization, we used an isotropic g value for all of the complexes. We also assumed that the rhombic parameter was equal to zero, even though this is probably not the case; however, magnetization of the Kramers ion is not very sensitive to a change of the rhombic parameter.[33] An excellent agreement between the fitted and experimental data with the parameters presented in Table 1 was obtained. The errors observed in the extracted parameters are given in Figure S6. The parameters are consistent with those reported for other tetrahedral cobalt(II) complexes.[46,56,59] The extracted SH parameters of the present series **1**–**3** are compared in Table 1 with those of the parent complexes (**1a**–**3a**).

Table 1. SH Parameters Extracted from *ORCA* (NEVPT2) and *PHI* Fittings for Complexes 1–3 and Their Parent Complexes 1a–3a

	ORCA			*PHI*		
complex	D_{cal} (cm^{-1})	g_x, g_y, g_z	$\lvert E/D\rvert$	D_{fit}(cm^{-1})	g_{iso}	TIP (cm^3 mol^{-1})
1	−18.9	2.26, 2.28, 2.39	0.09	−18.1	2.26	5×10^{-4}
2	−16.64	2.28, 2.32, 2.34	0.088	−16.4	2.33	1×10^{-3}
3	−21.74	2.5, 2.17, 2.31	0.22	−22.0	2.4	1×10^{-4}
1a	+17.4	2.16, 2.30, 2.41	0.25	+10.8	2.2, 2.2, 2.4	
2a	±14.9	2.18, 2.29, 2.42	0.32	−18.7	2.21	
3a	−18.3	2.19, 2.29, 2.46	0.25	−19.3	2.3	

For complexes **1** and **2**, only a negative D value yields a good fit (fitting simultaneously both the magnetization and susceptibility data), while changing the sign of D (negative to positive) leads to a poor fit (data not shown). This unequivocally suggests that both **1** and **2** possess an Ising-type anisotropy with an easy axis of magnetization. For **3**, an excellent fit of the magnetization data can be obtained with both positive and negative D values. The insensitivity of the data to the sign of D in **3** arises likely from the large rhombicity that may be due to the significant structural distortion in **3** compared to **1** and **2**. Usually, bulk magnetic susceptibility studies yield only rough information on the magnitude and sign

DOI: 10.1021/acs.inorgchem.8b00160
Inorg. Chem. 2018, 57, 3371–3386

of D. Single-crystal magnetic susceptibility and/or torque studies are more appropriate;[60] however, when the crystal have molecules with different orientations, analysis of the data may not be unique.[33] Although both positive and negative D values reproduce the experimental magnetic data of **3** satisfactorily, the negative sign of D was unequivocally confirmed by the X-band EPR spectrum recorded at 5 K (vide infra). The trend observed (**3** > **1** > **2**) in the D values of complexes **1**−**3** is slightly changed from the expected order **3** > **2** > **1** usually found when molecules with very close structure are compared;[61] this is rationalized by ab initio calculations (vide Infra). It is worth noting that an inversion of the trend, from the "expected" behavior in the magnitude of the magnetic anisotropy of trigonal cobalt(II) complexes,[26,28] was observed and rationalized to be due to relatively large distortion in the equatorial plane of the trigonal-bipyramidal complexes.[24]

Table 1 clearly exemplifies that there is no change in the sign of D extracted for complexes **2** (D = −16.4 cm^{-1}) and **3** (D = −22 cm^{-1}) compared to their corresponding parent complexes **2a** (D = −18.7 cm^{-1}) and **3a** (D = −19.3 cm^{-1}), respectively; however, there is a slight change in the magnitude of the D value noticed (*PHI* fitting parameters). We point out that the D value extracted for these complexes (**1**−**3**) with an assumption of E = 0 (but this may not be the real scenario) and, hence, a quantitative comparison is not valid. We will rely on the results of the calculations to analyze the effect of distortion and its impact on D and E. In contrast to **2** or **3**, in **1** (D = −18.1 cm^{-1}), there is a change in not only the magnitude of D but also the sign of D compared to its parent analogue **1a** (D = +10.8 cm^{-1}). The drastic changes in the SH parameters of **1**−**3** compared to their parent analogues are due to substitution on the thiourea ligand (L), which induces structural distortion in the resulting cobalt(II) complexes. The rationale for these observations and the change in the electronic structure (responsible for this observed change in the SH for **1**−**3**) are detailed with the help of computational calculations (vide infra).

X-Band EPR Study of Polycrystalline Samples of 1−3. Although commercial X- or Q-band continuous-wave electron paramagnetic resonance (CW-EPR) spectroscopy cannot be used to quantitatively predict the magnitude of the D values ($D \gg h\nu$) for **1**−**3**, it can be used to predict/prove the sign of D. In order to support the SH parameters extracted from the magnetic data, variable-temperature X-band EPR measurements were performed on polycrystalline samples of **1**−**3**. All three complexes were found to be EPR-silent at 100 K, measured on polycrystalline samples. This feature likely arises because of the intrinsic fast relaxation associated with high-spin cobalt(II) complexes and/or complexes stabilized with easy-axis anisotropy. To avoid this complication, EPR measurements were performed on pure polycrystalline samples of all of the complexes at 5 K. As observed at 100 K, complex **1** was found to be EPR-silent; for **2** and **3**, broad parallel-type EPR signals occurred at an effective g value of >5 (Figure S7), while perpendicular signals were absent. The observed EPR spectra for **2** and **3** can be interpreted by considering an effective spin ground-state doublet $S = {}^1/_2$, and the observation of only the $g_{\|}$ transition affirmatively supports the easy-axis-type anisotropy for the cobalt(II) ion in these complexes. The observation of EPR signals for **2** and **3** at 5 K also proves that the complex possesses nonzero rhombic anisotropy, which is strongly corroborated with the theoretical calculations (vide infra).

The presence of dipolar interaction often leads to the smearing of hyperfine interaction, which prevents the extraction of any meaningful parameters from the EPR spectrum. In order to reduce dipolar interaction, X-band EPR was measured on a diluted solid solution of $[Zn_{0.98}Co_{0.02}(L_1)_2(X)_2]$, where X = Cl (**1-dil**), Br (**2-dil**), and I (**3-dil**) at 5 K. Similar to the pure crystalline sample of **1**, **1-dil** remains EPR-silent at 5 K. On the other hand, unlike the pure crystalline solids of **2** and **3**, both **2-dil** and **3-dil** show well-resolved EPR signals (Figure 5). This

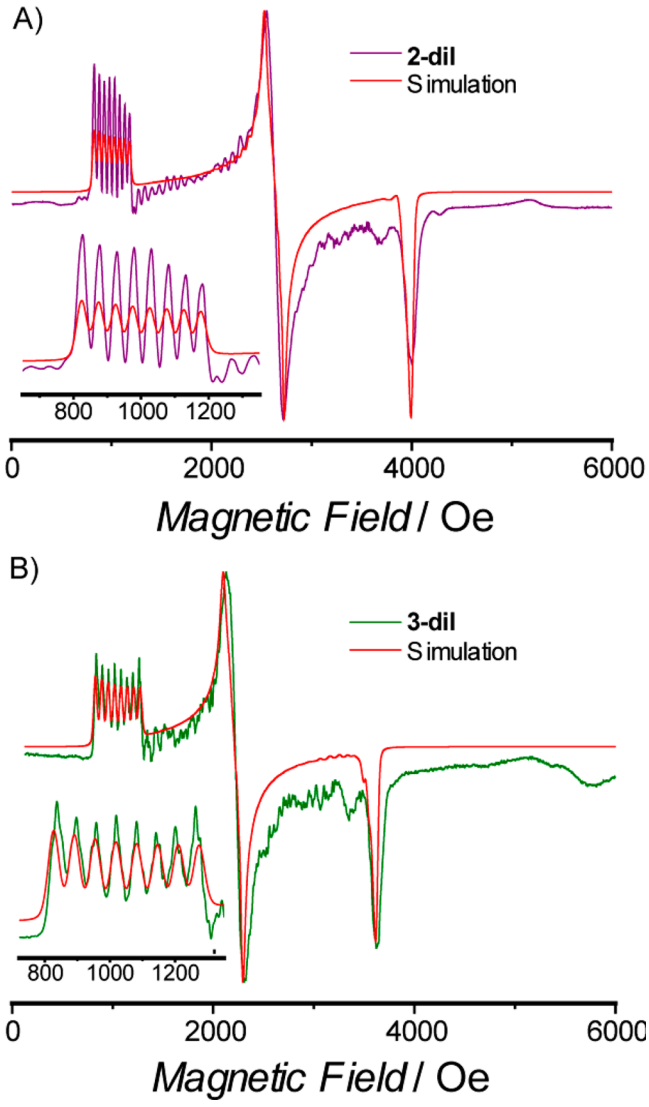

Figure 5. X-band EPR spectra of diluted solid solutions of complexes **2-dil** (panel A) and **3-dil** (panel B) recorded at 5 K. The insets on both panels show the expanded regions of the g_z^{eff} signals of the corresponding complexes. Microwave power = 20 dB (2 mW), modulation amplitude = 0.4 mT, and microwave frequency = 9.3834 GHz (for **2-dil**) and 9.3985 GHz (for **3-dil**).

clearly emphasizes the influence of dipolar interactions, which might have a significant influence in the opening of other relaxation pathways in ac data. Three well-resolved EPR signals are observed for both **2-dil** and **3-dil** complexes. The experimental EPR spectrum was simulated satisfactorily by considering an effective spin ground-state doublet $S = {}^1/_2$ and hyperfine interactions of cobalt for both cases with g_z^{eff} = 6.70, g_y^{eff} = 2.55, and g_x^{eff} = 1.680 and A_z = 473 MHz, A_y = 85 MHz,

DOI: 10.1021/acs.inorgchem.8b00160
Inorg. Chem. 2018, 57, 3371−3386

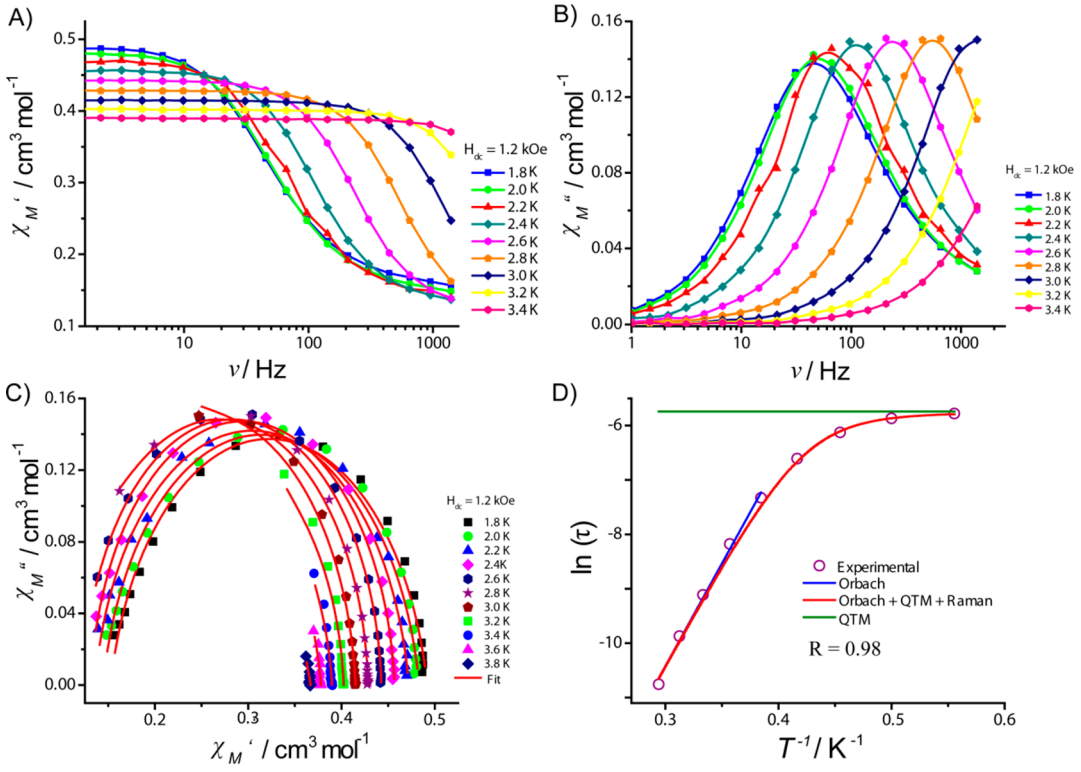

Figure 6. Frequency dependence of the (A) in-phase component, (B) out-of-phase component of the ac susceptibility, (C) Cole−Cole plot measured at the indicated external bias field, and (D) Arrhenius plot constructed by τ values extracted through Cole−Cole plot fitting for a 100% sample of complex **1**. The solid red lines in panels C and D represent the best fits obtained for the data using the parameters described in the main text.

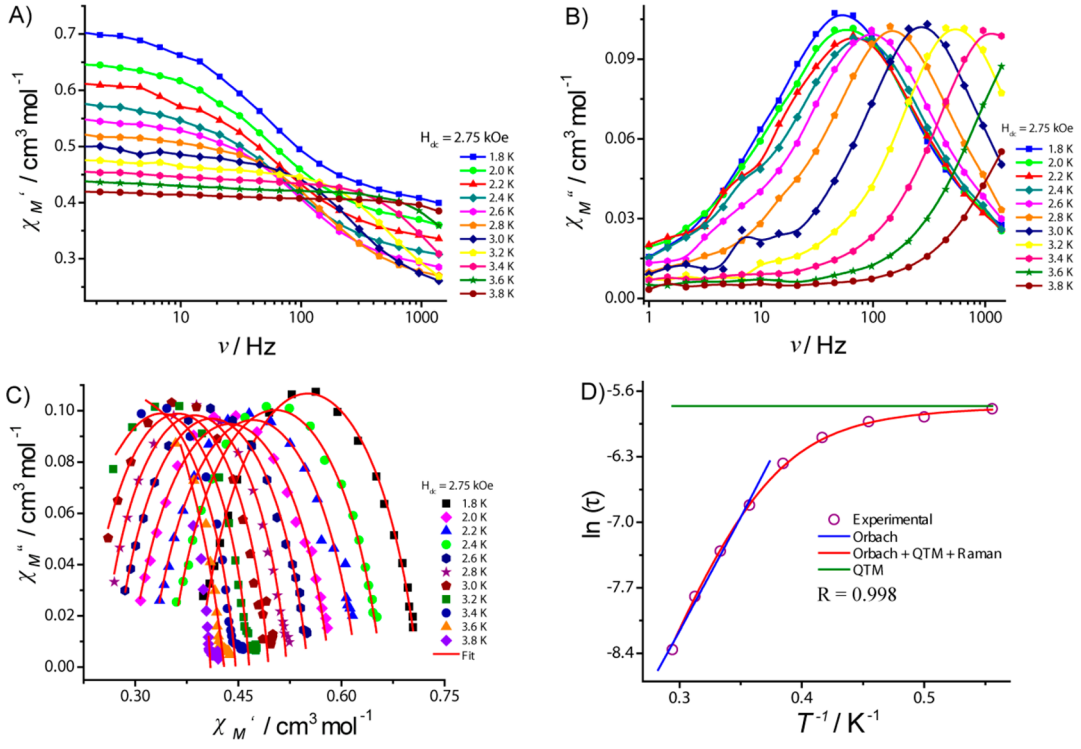

Figure 7. Frequency dependence of the (A) in-phase component, (B) out-of-phase component of the ac susceptibility, (C) Cole−Cole plot measured at the indicated external bias field, and (D) Arrhenius plot constructed by τ values extracted through Cole−Cole plot fitting for a 100% sample of complex **2**. The solid red lines in panels C and D represent the best fits obtained for the data using the parameters described in the main text.

DOI: 10.1021/acs.inorgchem.8b00160
Inorg. Chem. 2018, 57, 3371−3386

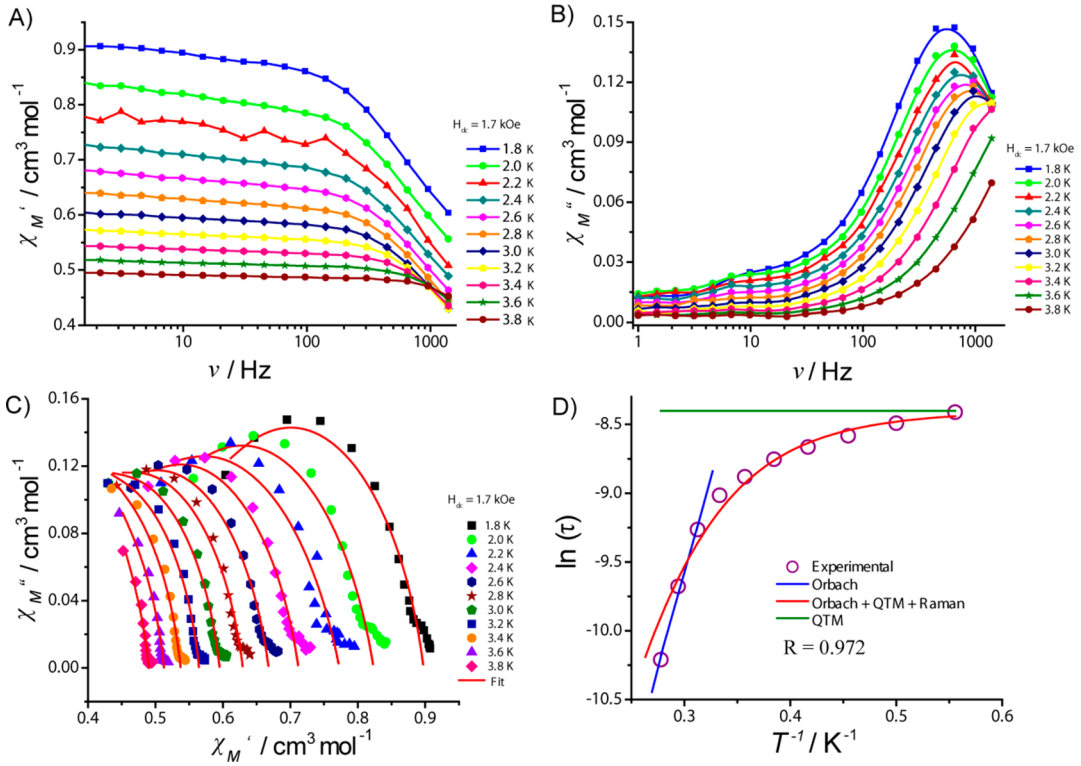

Figure 8. Frequency dependence of the (A) in-phase component, (B) out-of-phase component of the ac susceptibility, (C) Cole−Cole plot measured at the indicated external bias field, and (D) Arrhenius plot constructed by τ values extracted from Cole−Cole plot fitting for a 100% sample of complex **3**. The solid red lines in panels C and D represent the best fits obtained for the data using the parameters described in the main text.

and A_x = 10 MHz (for **2-dil**) and g_z^{eff} = 6.690, g_y^{eff} = 3.05, and g_x^{eff} = 1.87 and A_z = 570 MHz, A_y = 100 MHz, and A_x = 20 MHz (for **3-dil**) (Figure 5). The observation of $g_z^{eff} \gg g_y^{eff}$ and g_x^{eff} in both cases (**2-dil** and **3-dil**) unambiguously reveals the easy-axis-type anisotropy of cobalt(II) ions in both complexes **2** and **3**. This is consistent with other literature reports.[32,62−65] Overall, the X-band EPR measurements performed at 5 K on both the pure crystalline sample and diluted solid solution of all of the complexes (**1**−**3**) unmistakably disclose the Ising-type easy-axis anisotropy associated with cobalt(II) ions, which is consistent with the sign of D extracted from dc magnetic data fitting.

ac Magnetic Susceptibility Measurements of 1−3. Analysis of the magnetic data reveals the presence of an Ising-type magnetic anisotropy in complexes **1**−**3**; ac susceptibility studies were thus carried out for the pure samples and complexes diluted in the zinc(II) diamagnetic compound in order to assess the relaxation behavior of their magnetization. The measurements were performed between 2 and 8 K in the presence of a 3 Oe ac oscillating field at frequencies ranging from 1 to 1500 Hz in the presence and absence of an external optimum static dc magnetic field. In the absence of an external dc field, no out-of-phase susceptibility signals are observed apart from a tiny χ_M'' signal for **2** at T = 1.8 K and frequencies larger than 1000 Oe.

In order to identify the field at which relaxation becomes slower, we performed field-dependent ac measurements at T = 1.8 K and dc fields ranging from 0 to 3 kOe (Figure S8). The optimum fields were found to be equal to 1.2, 2.75, and 1.7 kOe for **1**−**3**, respectively. ac measurements were then performed under an optimum dc external magnetic field for the three complexes. The in-phase, out-of-phase, and corresponding Cole−Cole [$\chi'' = f(\chi')$] plots are shown in Figures 6−8 for complexes **1**−**3**, respectively. The measurements show that they present slow relaxation of magnetization because of the presence of frequency-dependent in-phase and out-of-phase signals that could be analyzed using the generalized Debye model. The data were fitted by considering a single relaxation process using the generalized Debye model (eq 2), where χ_S = adiabatic susceptibility, χ_T = isothermal susceptibility, ω = angular frequency, τ = relaxation time, and α reflects the extent of distribution of the relaxation times.

$$\chi_{ac}(\omega) = \chi_S + \frac{\chi_T - \chi_S}{1 + (\iota\omega\tau)^{1-\alpha}} \quad (2)$$

The α values that range from 0.12 to 0.07 (for **1**), from 0.26 to 0.1 (for **2**), and from 0.28 to 0.15 (for **3**) imply a narrow distribution of relaxation times in all of the complexes (Tables S3−S5). The τ values extracted from the Cole−Cole fits were used to construct the Arrhenius plot for all of the complexes. The Arrhenius plot deviates from linearity below 2.6−3.0 K in all three complexes. The nonlinearity in the Arrhenius plot is due to other competing relaxation processes such as Raman, direct, and quantum tunneling of magnetization (QTM) pathways apart from the temperature-dependent Orbach process.

We have fitted the $\ln(\tau) = f(1/T)$ curves in the entire temperature range considering the relaxation processes given below (eq 3). The first term on the right side of eq 3 represents the QTM process, the second term denotes the direct process, the third term is the Raman process, and the final one corresponds to the Orbach process.

DOI: 10.1021/acs.inorgchem.8b00160
Inorg. Chem. 2018, 57, 3371−3386

$$\frac{1}{\tau} = \frac{1}{\tau_{QTM}} + AH^2T + CT^n + \frac{1}{\tau_0}\exp\left(\frac{-U_{eff}}{k_BT}\right) \quad (3)$$

It is observed that it is not mandatory to employ all of the relaxation processes listed in eq 3. Just by employment of QTM, the Raman and Orbach processes yield excellent fits to the experimental data [$\ln(\tau) = f(1/T)$]. The parameters extracted by fitting the Arrhenius curves for all three complexes are listed in Table 2.[66−68] Note here that the direct process is not included in the fit; this could be attributed to the fact that, for Kramers ions having two states with similar compositions of the wave function, the transition element is likely to cancel out,[69] and this could be the reason why our data could fit well without the direct process, despite the fact that the data are measured in the presence of a field. However, the important message is that these pure complexes have slow relaxation through several relaxation processes, which could be qualitatively apprehended by examining the experimental $\ln(\tau) = f(1/T)$. Another remark can be made on the evolution of the maxima of the $\chi'' = f(\text{freq})$ curves with temperature. Upon cooling, the values of the maxima of the curves do not increase as expected for paramagnetic complexes; this is probably due to the presence of weak antiferromagnetic coupling in the temperature range 3−1.8 K, which could be due to hydrogen bonding or magnetic dipolar interactions. Thus, in order to gain better insight into the relaxation processes, we diluted the complexes in the diamagnetic zinc(II) compound [(10% cobalt(II) + 90% zinc(II)].

Table 2. Magnetization Relaxation Dynamics Parameters Extracted from Arrhenius Data Fits of Complexes 1−3 (100% Sample and 10% Diluted Samples)

	Orbach		Raman		QTM
complex	U_{eff}/cm^{-1} (H_{dc}/kOe)	τ_0/s	C/s^{-1} K^{-6}	N	τ_{QTM}/s
		100% Sample			
1	26.2 (1.2)	3.69×10^{-10}	0.221	6	0.0032
2	22.9 (2.75)	2×10^{-8}	0.402	6	0.00315
3	27.8 (1.7)	1.22×10^{-8}	5.7	6	0.00022
		10% Diluted Sample			
1	27.2 (1.1)	2.29×10^{-10}			
2	27.1 (0.7)	3.3×10^{-9}	0.048	6	0.021
3	32.7 (1.1)	2.29×10^{-10}	0.271	6	0.025

For the 10% diluted complexes, no out-of-phase signal is found except for **1** at T = 1.8 K and a frequency larger than 1000 Hz. The ac measurements were thus carried out in the presence of an optimum field for each compound that was found to be weaker than that of the nondiluted complexes (Figure S8). Examination of the out-of-phase curve (Figures 9−11, panel B) shows that the values of their maxima increase upon cooling, which is the expected behavior in the absence of antiferromagnetic coupling within the compounds.

Furthermore, the maxima of the $\chi'' = f(\nu)$ curves shift to lower frequencies upon cooling, showing that some relaxation processes present in the nondiluted compounds have now been suppressed or their contributions have decreased. These experiments suggest that the slow relaxations of magnetization observed in the diluted compounds are due to the single-molecule origin of the rather collective bulk phenomena of complexes **1**−**3**.

Analysis of the ac data was carried out similarly to that for the nondiluted complexes; the fit parameters are listed in Tables

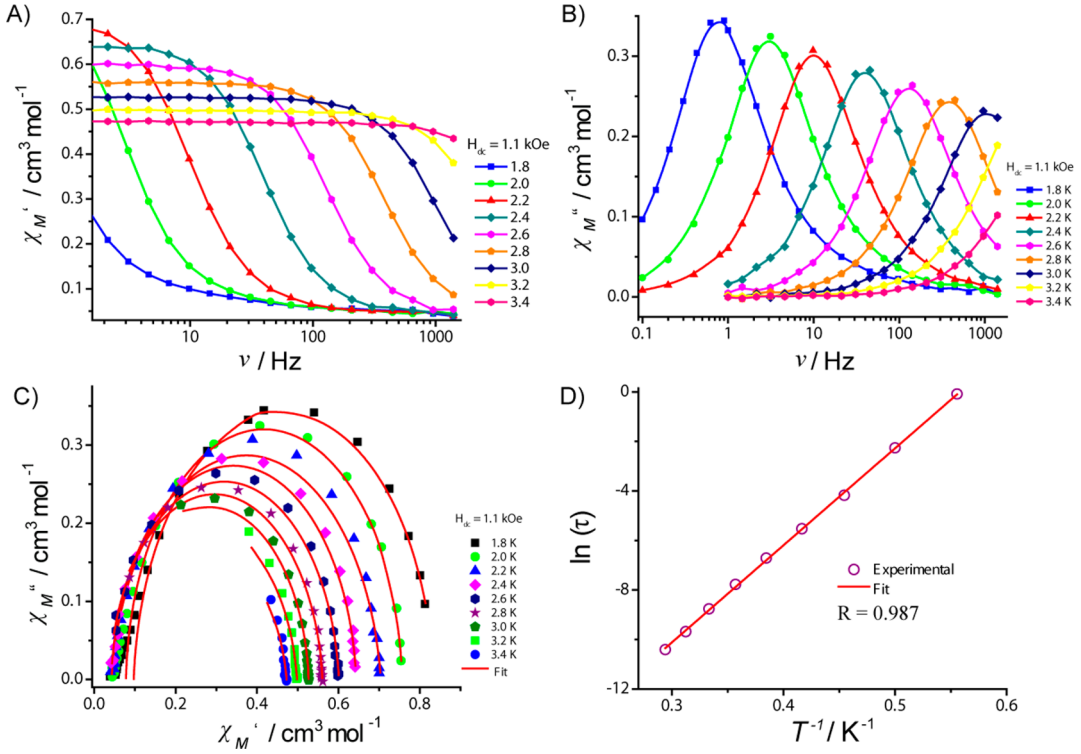

Figure 9. Frequency dependence of the (A) in-phase component, (B) out-of-phase component of the ac susceptibility, (C) Cole−Cole plot measured at the indicated external bias field, and (D) Arrhenius plot constructed by τ values extracted through Cole−Cole plot fitting for a 10% diluted sample of complex **1**.

DOI: 10.1021/acs.inorgchem.8b00160
Inorg. Chem. 2018, 57, 3371−3386

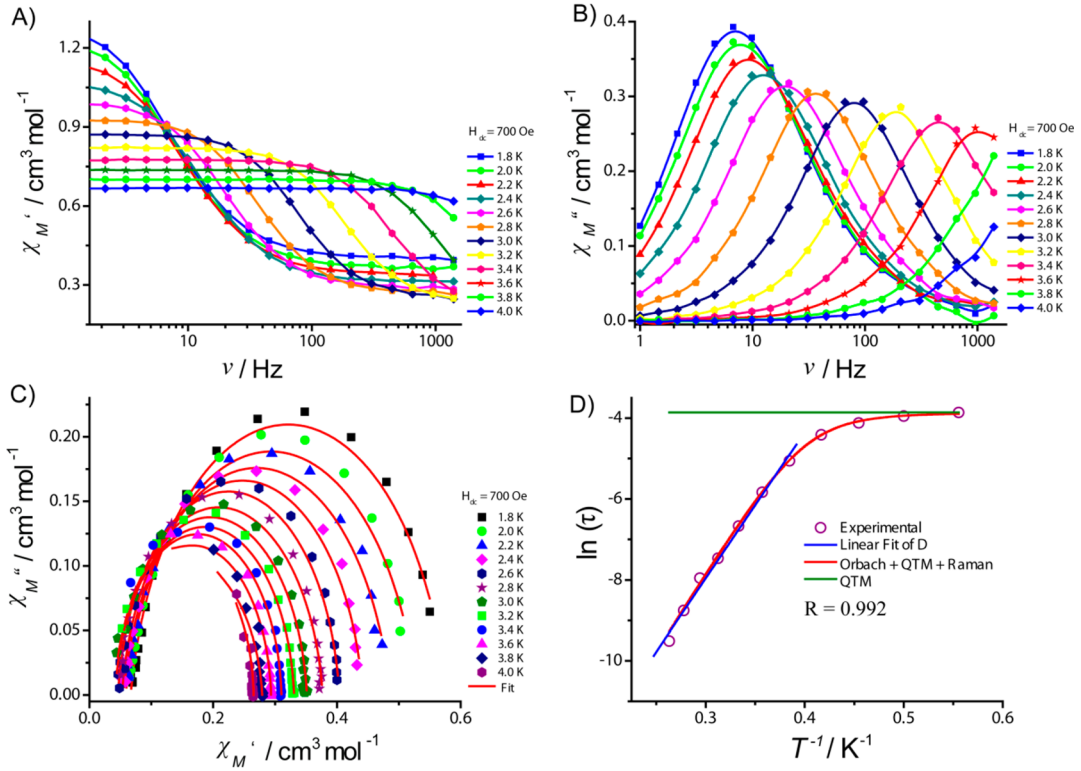

Figure 10. Frequency dependence of the (A) in-phase component, (B) out-of-phase component of the ac susceptibility, (C) Cole−Cole plot measured at the indicated external bias field, and (D) Arrhenius plot constructed by τ values extracted through Cole−Cole plot fitting for a 10% diluted sample of complex **2**.

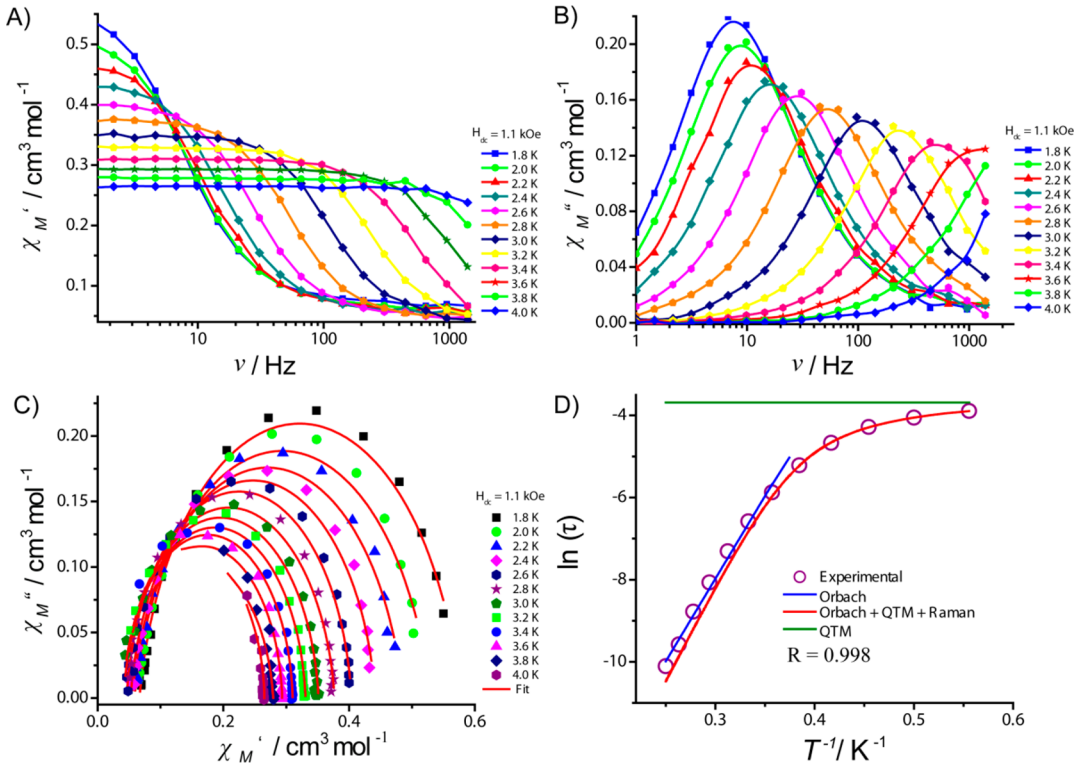

Figure 11. Frequency dependence of the (A) in-phase component, (B) out-of-phase component of the ac susceptibility, (C) Cole−Cole plot measured at the indicated external bias field, and (D) Arrhenius plot constructed by τ values extracted through Cole−Cole plot fitting for a 10% diluted sample of complex **3**.

S6−S8. The main difference concerns the relaxation times and their distributions (α). The relaxation time (τ) values are significantly longer for the diluted compounds, particularly for complex **1**, where an increase of 2 orders of magnitude (from

DOI: 10.1021/acs.inorgchem.8b00160
Inorg. Chem. 2018, 57, 3371−3386

Table 3. CASSCF- and NEVPT2-Computed SH Parameters (g, D, and $|E/D|$) along with the Listed State-by-State Contributions to the D Values

		1			2			3		
state		energy (cm^{-1})	contribution to D (cm^{-1})	contribution to E (cm^{-1})	energy (cm^{-1})	contribution to D (cm^{-1})	contribution to E (cm^{-1})	energy (cm^{-1})	contribution to D (cm^{-1})	contribution to E (cm^{-1})
					CASSCF					
$^4T_2(F)$		1935	−49.65	1.71	1753	−52.5	1.82	1240	−80.7	0.001
		2975	16.5	−17.4	2704	15.5	−8.76	2081	+15.8	24.02
		3024	8.4	13.6	2937	11.8	4.96	3503	6.9	1.97
	D_{tol}		−22.7		−22.14		−37.0			
	$\|E/D\|$		0.085		0.089		0.16			
	g_{xx}		2.36		2.45		2.5			
	g_{yy}		2.58		2.39		2.17			
	g_{zz}		2.33		2.49		2.31			
					NEVPT2					
$^4T_2(F)$		2806	−35.6	1.27	2682	−35.2	1.37	2261	−49.04	0.001
		4490	11.2	−11.4	4174	10.06	−6.4	3281	15.5	−15.8
		4575	5.8	8.8	4559	7.6	3.7	5667	4.26	1.2
	D_{tol}		−18.18		−16.52		−23.7			
	$\|E/D\|$		0.08		0.09		0.19			
	g_{xx}		2.25		2.32		2.31			
	g_{yy}		2.43		2.27		2.24			
	g_{zz}		2.23		2.35		2.48			

0.003 to 0.2 s) is observed. The distributions of the relaxation times are less important for the three complexes and particularly for complex **1** (0.04 at 1.8 K). For this complex, the $\ln(\tau) = f(1/T)$ curve (Figure 9D) is a straight line, suggesting that all relaxation processes apart from the Orbach one have been suppressed (or their contributions highly decreased) upon dilution.

The relaxation barriers (U_{eff}) extracted for the fit of the $\ln(\tau) = f(1/T)$ curves (Figures 9D, 10D, 11D and Table 2) are very close to those of the nondiluted complexes. For all complexes **1**−**3**, they are smaller than their corresponding theoretical values $2|D|$ (27, 27, and 33 cm^{-1} compared to 36, 33, and 44 cm^{-1} for **1**−**3**, respectively), which suggests that, even for complex **1**, where only an Orbach process is inferred from $\ln(\tau) = f(1/T)$, other processes are still active. There are several factors that might open up multiple relaxation processes in complexes, which reduces the effective energy barrier compared to the predicted one: (1) nuclear hyperfine interaction; (2) large E/D value facilitating QTM; (3) dipolar interaction; (4) weak antiferromagnetic coupling between the molecules. The influence of nuclear hyperfine interaction in magnetization relaxation dynamics of cobalt(II) was shown earlier by us.[32] The observation of EPR spectral features implies that the complexes possess nonzero "E" values, which is well supported by ab initio calculations. The presence of nonzero rhombic hyperfine interactions is very well witnessed experimentally (X-Band EPR section). All of these factors tend to reduce the effective energy barrier, and therefore the observed barrier height is much smaller than the theoretical estimate. To summarize the results of ac relaxation dynamics, the three complexes behave as SMMs with a relatively long relaxation time for the chloride-containing complex (**1**). Analysis of the structural data can be carried out considering the D values obtained for fitting of the dc magnetization data.

Theoretical Studies on Complexes 1−3. To estimate the magnetic anisotropy and to probe the origin of the difference in the D and E values observed in complexes **1**−**3**, we have undertaken ab initio calculations based on the CASSCF/NEVPT2 method using the *ORCA* suite of programs.[32,34,50,51] The computed SH parameters for complexes **1**−**3** are listed in Table 3. Using these parameters, the experimental magnetic data were simulated. The simulated data [$\chi_M T(T)$ and $M(B)$] are in excellent agreement with the experimental data (Figure 12). Besides, the obtained parameters are also consistent with

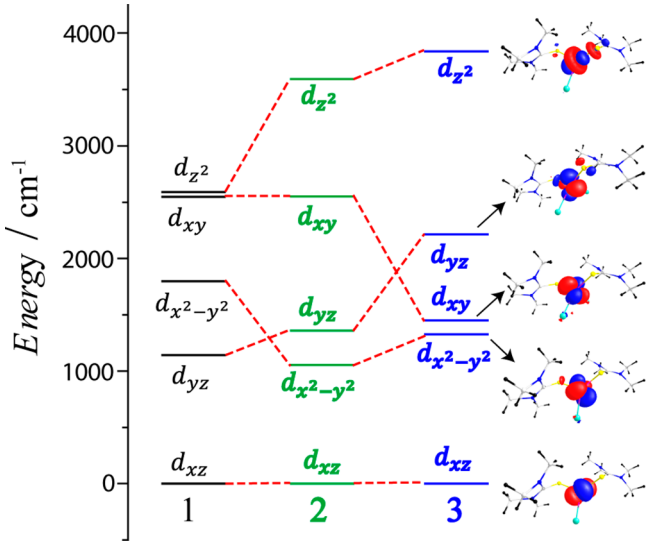

Figure 12. CASSCF-computed d-orbital energy ordering for complexes **1**−**3**.

the parameter set obtained using *PHI*. These multiple and independent types of extracted SH parameters increase confidence in the estimated parameters obtained.

Upon comparison of the computed data of the parent molecules **1a**−**3a** (Table S9) with **1**−**3** (Table 3), large variations are observed in the estimated g, D, and $|E/D|$ values. To understand this in detail, the crystal structures of both of the families (**1**−**3** and **1a**−**3a**) were analyzed carefully (Figure S9). Figure S9 unambiguously shows that the presence of

DOI: 10.1021/acs.inorgchem.8b00160
Inorg. Chem. 2018, 57, 3371−3386

substituents on the ligands brings significant distortion to the coordination sphere, and this distortion can be quantified in terms of $\delta = 2T_d - (\alpha + \beta)$ (where $T_d = 109.5°$ and α and β represent the S11−Co−S12 and X11−Co−X12 angles, respectively, in complexes **1**−**3** and **1a**−**3a**). As was stated earlier by us on a related molecule,[34,70] the positive value of δ suggests that cobalt(II) is tetragonally elongated, while the negative value signifies that cobalt(II) acquires a flattened tetrahedron (toward a square-planar) geometry. Calculations reveal that complexes **1**−**3** have negative δ values, while their parent complexes possess positive δ values (Table S10). Alteration from tetragonal elongation to a flattened tetrahedron in **1**−**3** is brought by the substituents on the thiourea ligand. This effect is expected to significantly influence the electronic structure of the complexes and, consequently, their magnetic anisotropy. Among the complexes **1**−**3**, **3** possesses the largest negative δ value; hence, its symmetry is lower than those of **1** and **2**. This is in accordance with the large $|E/D|$ value computed for **3** compared to **1** or **2**.

Although all of the complexes appear to be in the pseudotetrahedral geometry, they actually possess only a pseudo-C_2 symmetry considering only the first coordination sphere. The electronic state spectroscopic terms obtained considering ligand-field theory for the cobalt(II) ion in T_d symmetry are $^4A_2(F)$, $^4T_2(F)$, and $^4T_1(P)$. They split into ^4A, [^4A, and two ^4B](F) and [^4A and two ^4B](P) states, respectively, in C_2 symmetry. The ^4A term arising from $^4A_2(F)$ becomes the ground state, while the three states (^4A and two ^4B terms) arising from the $^4T_2(F)$ term become the first three excited states. The various transitions that contribute to the overall D value for each complex are listed in Table 3. It has been well established that the spin-conserved transition between orbitals having the same m_l values contributes to the negative D value, while the transition between the orbitals of two different m_l values contributes to the positive D value.[18,27,29,30,32,34,71] The spin-conserved lowest-energy transition in all three complexes is observed for $^4A_1$ ($^4A_2$) → $^4A_2$ ($^4T_2$), which contributes to the negative D value.

As the energy gap between the ground state and the first excited state decreases as we move from **1** to **2** to **3**, the contribution to the negative D value increases in the same order. The spin-conserved transition from the ground state to the second and third excited states contributes to the positive D value, which actually tends to reduce the overall axial single-ion anisotropy of the molecules. Even though the positive contributions to D coming from the excited states are slightly larger for **3**, its computed D value remains more negative than those for **1** and **2** (Table 3). For the rhombic term E, the first excited states contribute very little, while the second and third excited ones contribute in the opposite way; i.e., the second one has a negative contribution and the third a positive one. The large overall E value for complex **3** is due to the large difference in the contributions of the second and third excited states, while this is not the case for **1** and **2** (Table 3, NEVPT2 calculations), leading to $|E/D|$ values of 0.08, 0.09, and 0.19 for **1**−**3**, respectively.

The difference in the anisotropy parameters between the two series of complexes (**1**−**3** and **1a**−**3a**) can be rationalized by comparing the contributions of each excited state to the overall parameter values and can then be correlated to their structural difference: flattened tetrahedra for **1**−**3** and tetragonal elongation for **1a**−**3a**. In the case of **1a**−**3a**, the first two excited states have positive contributions to D, and the third one has a negative contribution.

This is in absolute contrast with the D contribution arising from various transitions in **1**−**3**, and this explains why **1a** has an overall positive D value, while a negative D value is obtained for **1** (Table S8).

Further, we have analyzed the eigenvalue plots of complexes **1**−**3**, and how the orbital ordering changes upon changes to the halides is shown in Figure 12. While d_{z^2} and $d_{x^2-y^2}$ are found to be lower in energy compared to d_{xz}, d_{yz}, and d_{xy} in complexes **1a**−**3a** (Figure S10), a different scenario is noted here, where the d_{xz} orbital is found to be lower in energy and the d_{z^2} orbital is found to be higher in energy. However, calculations clearly reveal that the ground-state wave function has multideterminantal characteristics, and the representation in Figure 13 shows only a major contribution to the wave function.

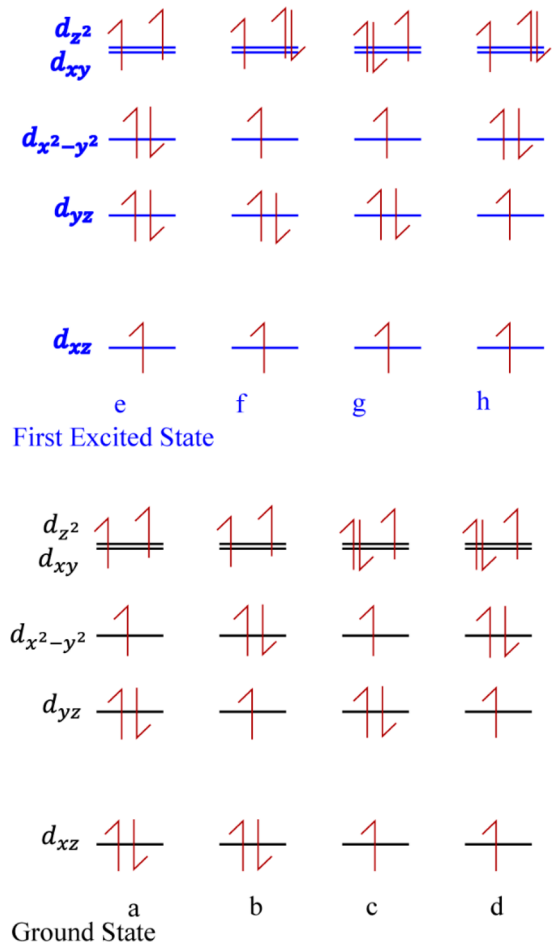

Figure 13. Multideterminant wave function of the ground (a = 0.5, b = 0.14, c = 0.12, and d = 0.10) and excited (e = 0.5, f = 0.26, g = 0.13, and h = 0.06) states of complex **1**. The computed CI coefficients that are larger than 5% are shown above.

This observed trend in **1**−**3** can be qualitatively explained on the basis of *the simultaneous effects* of the π-donor halides, the π-anisotropic sulfur interactions with the nonbonding orbital of cobalt(II) in the T_d geometry, and the structural distortion around the cobalt(II) ion in all of the complexes (**1**−**3**). Noticeably, the cobalt(II) ion in all three complexes possesses neither absolute tetrahedral symmetry nor square-planar geometry but possesses a geometry that is between the two.

DOI: 10.1021/acs.inorgchem.8b00160
Inorg. Chem. 2018, 57, 3371−3386

Table 4. NEVPT2-Computed SH Parameters (D and $|E/D|$) along with the Listed State-by-State Contributions to the D Values for 1 and Modeled Complexes 1-Br and 1-I

		1		1-Br		1-I	
state		energy (cm^{-1})	contribution to D (cm^{-1})	energy (cm^{-1})	contribution to D (cm^{-1})	energy (cm^{-1})	contribution to D (cm^{-1})
$^4T_2(F)$		2806	−35.6	2507	−38	2331	−40
		4490	11.2	4172	13	4079	10
		4575	5.8	4283	6.7	4233	10
	D_{tol}		−18.18		−17.1		−18.07
	$\|E/D\|$		0.08		0.06		0.03

This situation originates because of the substituent on the thiourea ligand compared to their parent complexes. Further, the substituent-induced structural distortion in **1**−**3** likely enables stronger π-donor interaction with metal nonbonding orbitals compared to **1a**−**3a**. Also it is well demonstrated in the literature that the π-donor ligand destabilizes the nonbonding orbitals ($d_{x^2-y^2}$ and d_{z^2}). The influence of various antibonding (σ and π for in-plane and out-of-plane) interactions of the π-anisotropic ligand and the geometry of a four-coordinate cobalt(II) ion upon determination of the sign and magnitude of D are elegantly explained by Neese and co-workers.[29,72] Therefore, the observed orbital ordering in **1**−**3** can be qualitatively attributed to the geometric distortions and the π interactions of halide and sulfur ligands (Figure S10).

For a high-spin cobalt(II) ion, on the basis of Figure 12, the lowest-energy transition will involve a change in the m_l value, which will stabilize the $\pm^1/_2$ Kramers state of the ground state. This, in fact, is opposite to the trend observed experimentally (X-band EPR data of **1**−**3** unmistakably confirm the easy-axis anisotropy associated with cobalt(II) ions and the parameters extracted from magnetic data) and the computed results. The reason for stabilization of the negative D value in these complexes is that both the ground and excited states are not pure but have multideterminant characteristics (Figure 13). In particular, the first excited state of complex **1**, which contributes −35.6 cm^{-1} (NEVPT2; see Table 3) to the net D value, increases, where one of the dominant contributions arises by a transition from d_{xz} to d_{yz} orbitals, as shown in Figure 13. A similar scenario is visible also for other complexes; however, mixing of the wave function is more rigorous for complexes **2** and **3** than for **1** (Figures S11 and S12).

To unravel the individual contributions of the distortion and nature of a halide linked to cobalt(II) to the overall D value in complexes **1**−**3**, we performed ab initio calculations on fictitious model complexes, which are derived from complex **1**, where Cl^- was replaced by Br^- (**1-Br**) and I^- (**1-I**). These models were constructed by altering only the Co−X bond lengths and keeping other structural parameters as such in complex **1**. This set of calculations reveals no appreciable change in the D value upon replacement of Cl^- by Br^- or I^- ions (Table 4). This is somewhat surprising and is in contradiction with other reports.[34,38,44] In order to understand this in more depth, the statewise contribution to D was analyzed carefully (Table 4). Table 4 distinctly shows the effect of heavier halides on various energy levels; i.e., the excited states are much closer to the ground states in **1-Br** and **1-I** compared to **1**. This is as expected for the weaker ligand-field interaction of −Br or −I with the cobalt(II) ion. Thus, the energy levels are indeed altered upon changes in Cl^- by Br^- or I^-.

Besides, we noticed that there is an increase of the negative D contribution due to the lowest-energy excitation as we go from complexes **1** to **1-Br** to **1-I** (Table 4). On the other hand, the remaining two excitations responsible for the positive D contributions also increase in **1-Br** and **1-I** compared to **1**. As a result, the increased negative D contribution is clearly nullified by the increase in the positive D contributions in the **1-Br** and **1-I** model complexes. This evidently emphasizes that the distortion induced by the substituent also contributes to the D value. To further understand how distortion plays a role in governing the D value, we have developed a magnetostructural correlation for the δ parameter.

Further, in order to qualitatively predict the sign and magnitude of D in structurally analogous complexes like **1**−**3**, we have developed a magnetostructural correlation on all three complexes by varying the δ value from −50° to +50°. In all three complexes, the computed D value is observed to be large when δ = −50°. Upon going from flattened tetrahedral geometry to ideal tetrahedral geometry (increasing δ value), the overall axiality of the computed D value decreases (Figure 14A). The sign of the D value changes from negative to positive when the geometry changes to an elongated tetrahedron. For example, when δ = +20°, an overall positive D value is witnessed for all three complexes. However, the sign of the computed D unambiguously could not be determined in the range of δ = +20° to +30° because the $|E/D|$ value is close to 0.30. A further increase in the δ value beyond +30 again stabilizes the easy-axis anisotropy (Figure 14A). The D values obtained through the developed correlation for all three complexes well correlated to the energy gap between the ground and first excited states. As stated earlier, the lowest-energy transition contributes significantly to the overall D value, which is typically inversely proportional to the energy gap between the ground and first excited states. This energy gap is small when δ = −50°, which gradually increases with an increase in the δ value (Figure 14B) for all three complexes. Thus, it rationalizes the trend observed in the computed D value. For complex **3** with a negative δ value beyond 30°, the decrease in the energy gap does not follow the trend observed for compounds **1** and **2** (see the crisscross behavior in Figure 14B). Upon closer observation, we noted that, for these structures, a weak interaction between the iodine and sulfur atoms exists. This interaction tends to alter the donor capabilities of sulfur, leading to unusual behavior compared to that of complexes **2** and **3**. In order to validate the correlation developed, the D value extracted for **1**−**3** from a magnetic data fitting (using *PHI*) was mapped onto the correlation developed for all of the complexes. The excellent agreement between the correlation developed and the D value extracted from the magnetic data indeed implies reliability of the correlation developed (Figure 14). This emphasizes the importance of structural distortion in determining both the sign and magnitude of D, which are induced by the substituent on the thiourea ligand. We believe that the developed correlation

DOI: 10.1021/acs.inorgchem.8b00160
Inorg. Chem. 2018, 57, 3371−3386

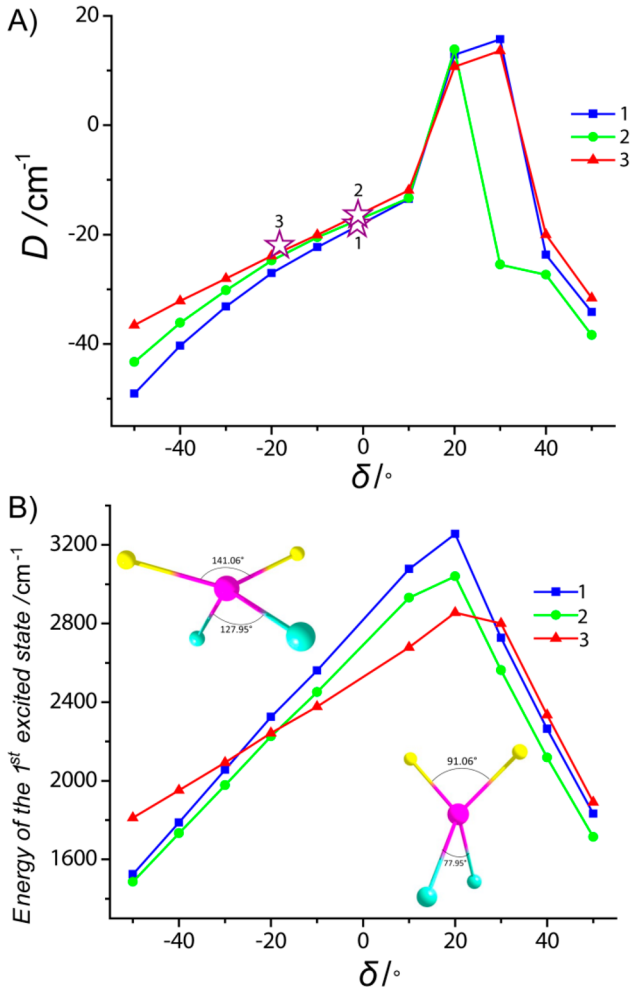

Figure 14. (A) Variation of the D values for complexes **1**−**3** by changing the δ angle. The D values obtained through the fitting are mapped on the correlation (open circles). (B) Energy variation of the first excited state originating from ^4T with respect to the change in the δ value. The graphs constructed here are based on the values computed at the CASSCF level of theory.

will be particularly useful for synthetic chemists to qualitatively predict the D value of the pseudotetrahedral complexes.

CONCLUSION

In conclusion, a family of pseudotetrahedral complexes with the general molecular formula $[Co(L_1)X_2]$ [X = Cl (**1**), Br (**2**), and I (**3**)] were isolated. dc and ac magnetic susceptibility studies were performed on all of the complexes. Substitution on the thiourea ligand brought visible geometric change from tetragonal elongation to a flattened tetrahedron in **1**−**3** compared to their parent complexes **1a**−**3a**. This change in geometry drastically changed the electronic structure and related SH parameters. The changes in the SH parameters were clearly reflected in the magnetization relaxation behavior. The origin of SIM behavior in these complexes was further confirmed by magnetic dilution studies. Ab initio calculations were employed to rationalize the observed dc and ac behavior in **1**−**3**. Calculations performed on complexes **1**−**3** and their related model complexes suggest that both the substituent and halide ion significantly alter the energy levels, leading to a large variation in the sign and magnitude of the D value. The present study reveals that, by simply changing the substituents on the ligand, one can significantly modulate the D and $|E/D|$ values, which is useful information for chemists involved in the design of SIMs because this offers a rather viable approach to reduce the $|E/D|$ value and enhancing the relaxation time.

ASSOCIATED CONTENT

Supporting Information

The Supporting Information is available free of charge on the ACS Publications website at DOI: 10.1021/acs.inorgchem.8b00160.

Crystallographic parameters, PXRD profiles, table of atoms involved in hydrogen bonding for all of the complexes, bond-length comparison of complexes **1**−**3** with their parent complexes (**1a**−**3a**), reduced magnetization data, VT EPR spectra, field-sweep ac relaxation dynamics for pure and magnetically diluted samples, Cole−Cole fitting parameters, related computed SH parameters, and eigenvalue plot for the relevant complexes (PDF)

Accession Codes

CCDC 1817777−1817779 contain the supplementary crystallographic data for this paper. These data can be obtained free of charge via www.ccdc.cam.ac.uk/data_request/cif, or by emailing data_request@ccdc.cam.ac.uk, or by contacting The Cambridge Crystallographic Data Centre, 12 Union Road, Cambridge CB2 1EZ, UK; fax: +44 1223 336033.

AUTHOR INFORMATION

Corresponding Authors

*E-mail: talal.mallah@u-psud.fr.
*E-mail: rajaraman@chem.iitb.ac.in.
*E-mail: eswar@chem.iitb.ac.in. Phone/Fax: +91-22-2576-7187/+91-22-2576-7152.

ORCID

Talal Mallah: 0000-0002-9311-3463
Gopalan Rajaraman: 0000-0001-6133-3026
Maheswaran Shanmugam: 0000-0002-9012-743X

Notes

The authors declare no competing financial interest.

ACKNOWLEDGMENTS

M.S. thanks the funding agencies SERB (EMR/2015/000592) and INSA (SP/YSP/119/2015/1264) for financial support and the IIT Bombay-RIFC EPR central facility. S.V. and P.S. thanks CSIR for financial support. S.T. thanks IIT Bombay for financial support. G.R. thanks SERB-DST (EMR/2014/000247), INSA, for funding.

REFERENCES

(1) Sessoli, R.; Gatteschi, D.; Caneschi, A.; Novak, M. A. Magnetic bistability in a metal-ion cluster. *Nature* **1993**, *365*, 141−3.

(2) Caneschi, A.; Gatteschi, D.; Sessoli, R.; Barra, A. L.; Brunel, L. C.; Guillot, M. Alternating current susceptibility, high field magnetization, and millimeter band EPR evidence for a ground S = 10 state in $[Mn_{12}O_{12}(CH_3COO)_{16}(H_2O)_4].2CH_3COOH.4H_2O$. *J. Am. Chem. Soc.* **1991**, *113*, 5873−4.

(3) Bao, S.-S.; Zheng, L.-M. Magnetic materials based on 3d metal phosphonates. *Coord. Chem. Rev.* **2016**, *319*, 63−85.

(4) Murrie, M. Cobalt(II) single-molecule magnets. *Chem. Soc. Rev.* **2010**, *39*, 1986−1995.

(5) Neese, F.; Pantazis, D. A. What is not required to make a single molecule magnet. *Faraday Discuss.* **2011**, *148*, 229−238.

DOI: 10.1021/acs.inorgchem.8b00160
Inorg. Chem. 2018, 57, 3371−3386

(6) Abbasi, P.; Quinn, K.; Alexandropoulos, D. I.; Damjanovic, M.; Wernsdorfer, W.; Escuer, A.; Mayans, J.; Pilkington, M.; Stamatatos, T. C. Transition Metal Single-Molecule Magnets: A {Mn31} Nanosized Cluster with a Large Energy Barrier of ~ 60 K and Magnetic Hysteresis at ~ 5 K. *J. Am. Chem. Soc.* **2017**, *139*, 15644−15647.
(7) Sheikh, J. A.; Jena, H. S.; Clearfield, A.; Konar, S. Phosphonate Based High Nuclearity Magnetic Cages. *Acc. Chem. Res.* **2016**, *49*, 1093−1103.
(8) Lamouchi, M.; Jeanneau, E.; Novitchi, G.; Luneau, D.; Brioude, A.; Desroches, C. Polynuclear Complex Family of Cobalt(II)/Sulfonylcalixarene: One-Pot Synthesis of Cluster Salt $[Co_{14}^{II}]+[Co_4^{II}]$- and Field-Induced Slow Magnetic Relaxation in a Six-Coordinate Dinuclear Cobalt(II)/Sulfonylcalixarene Complex. *Inorg. Chem.* **2014**, *53*, 63−72.
(9) Lydon, C.; Sabi, M. M.; Symes, M. D.; Long, D.-L.; Murrie, M.; Yoshii, S.; Nojiri, H.; Cronin, L. Directed assembly of nanoscale Co(II)-substituted $\{Co_9[P_2W_{15}]_3\}$ and $\{Co_{14}[P_2W_{15}]=\}$ polyoxometalates. *Chem. Commun.* **2012**, *48*, 9819−9821.
(10) Taguchi, T.; Wernsdorfer, W.; Abboud, K. A.; Christou, G. Mn7 and Mn12 Clusters From Use of 2-(Pyridine-2-yl)propan-2-ol: A New Half-Integer Single-Molecule Magnet. *Inorg. Chem.* **2010**, *49*, 199−208.
(11) Hoshino, N.; Ako, A. M.; Powell, A. K.; Oshio, H. Molecular Magnets Containing Wheel Motifs. *Inorg. Chem.* **2009**, *48*, 3396−3407.
(12) Stamatatos, T. C.; Poole, K. M.; Abboud, K. A.; Wernsdorfer, W.; O'Brien, T. A.; Christou, G. High-spin Mn_4 and Mn_{10} molecules: large spin changes with Structure in mixed-valence MnII4MnIII6 clusters with azide and alkoxide-based ligands. *Inorg. Chem.* **2008**, *47*, 5006−5021.
(13) Ding, Z.-Y.; Meng, Y.-S.; Xiao, Y.; Zhang, Y.; Zhu, Y.-Y.; Gao, S. Probing the influence of molecular symmetry on magnetic anisotropy of octahedral cobalt(II) complexes. *Inorg. Chem. Front.* **2017**, *4*, 1909−1916.
(14) Deng, Y.-F.; Han, T.; Yin, B.; Zheng, Y.-Z. On balancing the QTM and the direct relaxation processes in single-ion magnets - the importance of symmetry control. *Inorg. Chem. Front.* **2017**, *4*, 1141−1148.
(15) Schweinfurth, D.; Krzystek, J.; Atanasov, M.; Klein, J.; Hohloch, S.; Telser, J.; Demeshko, S.; Meyer, F.; Neese, F.; Sarkar, B. Tuning Magnetic Anisotropy Through Ligand Substitution in Five-Coordinate Co(II) Complexes. *Inorg. Chem.* **2017**, *56*, 5253−5265.
(16) Craig, G. A.; Murrie, M. 3d single-ion magnets. *Chem. Soc. Rev.* **2015**, *44*, 2135−2147.
(17) Bar, A. K.; Pichon, C.; Sutter, J.-P. Magnetic anisotropy in two- to eight-coordinated transition-metal complexes: Recent developments in molecular magnetism. *Coord. Chem. Rev.* **2016**, *308*, 346−380.
(18) Gomez-Coca, S.; Aravena, D.; Morales, R.; Ruiz, E. Large magnetic anisotropy in mononuclear metal complexes. *Coord. Chem. Rev.* **2015**, *289−290*, 379−392.
(19) Harman, W. H.; Harris, T. D.; Freedman, D. E.; Fong, H.; Chang, A.; Rinehart, J. D.; Ozarowski, A.; Sougrati, M. T.; Grandjean, F.; Long, G. J.; Long, J. R.; Chang, C. J. Slow Magnetic Relaxation in a Family of Trigonal Pyramidal Iron(II) Pyrrolide Complexes. *J. Am. Chem. Soc.* **2010**, *132*, 18115−18126.
(20) Zadrozny, J. M.; Long, J. R. Slow Magnetic Relaxation at Zero Field in the Tetrahedral Complex $[Co(SPh)_4]_2$. *J. Am. Chem. Soc.* **2011**, *133*, 20732−20734.
(21) Ruamps, R.; Batchelor, L. J.; Maurice, R.; Gogoi, N.; Jiménez-Lozano, P.; Guihéry, N.; de Graaf, C.; Barra, A.-L.; Sutter, J.-P.; Mallah, T. Origin of the Magnetic Anisotropy in Heptacoordinate NiII and CoII Complexes. *Chem. - Eur. J.* **2013**, *19*, 950.
(22) Brazzolotto, D.; Gennari, M.; Yu, S.; Pécaut, J.; Rouzières, M.; Clérac, R.; Orio, M.; Duboc, C. An Experimental and Theoretical Investigation on Pentacoordinated Cobalt(III) Complexes with an Intermediate S = 1 Spin State: How Halide Ligands Affect their Magnetic Anisotropy. *Chem. - Eur. J.* **2016**, *22*, 925.
(23) Suturina, E. A.; Nehrkorn, J.; Zadrozny, J. M.; Liu, J.; Atanasov, M.; Weyhermueller, T.; Maganas, D.; Hill, S.; Schnegg, A.; Bill, E.; Long, J. R.; Neese, F. Magneto-Structural Correlations in Pseudotetrahedral Forms of the $[Co(SPh)_4]^{2-}$ Complex Probed by Magnetometry, MCD Spectroscopy, Advanced EPR Techniques, and ab Initio Electronic Structure Calculations. *Inorg. Chem.* **2017**, *56*, 3102.
(24) Shao, F.; Cahier, B.; Guihery, N.; Riviere, E.; Guillot, R.; Barra, A. L.; Lan, Y. H.; Wernsdorfer, W.; Campbell, V. E.; Mallah, T. Tuning the Ising-type anisotropy in trigonal bipyramidal Co(II) complexes. *Chem. Commun.* **2015**, *51*, 16475.
(25) Cahier, B.; Maurice, R.; Bolvin, H.; Mallah, T.; Guihéry, N. Tools for Predicting the Nature and Magnitude of Magnetic Anisotropy in Transition Metal Complexes: Application to Co(II) Complexes. *Magnetochemistry* **2016**, *2* (3), 31.
(26) Woods, T. J.; Ballesteros-Rivas, M. F.; Gómez-Coca, S.; Ruiz, E.; Dunbar, K. R. Relaxation Dynamics of Identical Trigonal Bipyramidal Cobalt Molecules with Different Local Symmetries and Packing Arrangements: Magnetostructural Correlations and ab inito Calculations. *J. Am. Chem. Soc.* **2016**, *138*, 16407.
(27) Gomez-Coca, S.; Cremades, E.; Aliaga-Alcalde, N.; Ruiz, E. Mononuclear Single-Molecule Magnets: Tailoring the Magnetic Anisotropy of First-Row Transition-Metal Complexes. *J. Am. Chem. Soc.* **2013**, *135*, 7010−7018.
(28) Ruamps, R.; Batchelor, L. J.; Guillot, R.; Zakhia, G.; Barra, A.-L.; Wernsdorfer, W.; Guihery, N.; Mallah, T. Ising-type magnetic anisotropy and single molecule magnet behaviour in mononuclear trigonal bipyramidal Co(II) complexes. *Chem. Sci.* **2014**, *5*, 3418−3424.
(29) Suturina, E. A.; Maganas, D.; Bill, E.; Atanasov, M.; Neese, F. Magneto-Structural Correlations in a Series of Pseudotetrahedral $[Co^{II}(XR)_4]^{2-}$ Single Molecule Magnets: An ab Initio Ligand Field Study. *Inorg. Chem.* **2015**, *54*, 9948−9961.
(30) Vaidya, S.; Upadhyay, A.; Singh, S. K.; Gupta, T.; Tewary, S.; Langley, S. K.; Walsh, J. P. S.; Murray, K. S.; Rajaraman, G.; Shanmugam, M. A synthetic strategy for switching the single ion anisotropy in tetrahedral Co(II) complexes. *Chem. Commun.* **2015**, *51*, 3739−3742.
(31) Sottini, S.; Poneti, G.; Ciattini, S.; Levesanos, N.; Ferentinos, E.; Krzystek, J.; Sorace, L.; Kyritsis, P. Magnetic Anisotropy of Tetrahedral CoII Single-Ion Magnets: Solid-State Effects. *Inorg. Chem.* **2016**, *55*, 9537−9548.
(32) Vaidya, S.; Tewary, S.; Singh, S. K.; Langley, S. K.; Murray, K. S.; Lan, Y.; Wernsdorfer, W.; Rajaraman, G.; Shanmugam, M. What Controls the Sign and Magnitude of Magnetic Anisotropy in Tetrahedral Cobalt(II) Single-Ion Magnets? *Inorg. Chem.* **2016**, *55*, 9564−9578.
(33) Cahier, B.; Perfetti, M.; Zakhia, G.; Naoufal, D.; El-Khatib, F.; Guillot, R.; Riviere, E.; Sessoli, R.; Barra, A.-L.; Guihery, N.; Mallah, T. Magnetic Anisotropy in Pentacoordinate NiII and CoII Complexes: Unraveling Electronic and Geometrical Contributions. *Chem. - Eur. J.* **2017**, *23*, 3648−3657.
(34) Vaidya, S.; Singh, S. K.; Shukla, P.; Ansari, K.; Rajaraman, G.; Shanmugam, M. Role of Halide Ions in the Nature of the Magnetic Anisotropy in Tetrahedral Co^{II} Complexes. *Chem. - Eur. J.* **2017**, *23*, 9546−9559.
(35) Yao, X.-N.; Du, J.-Z.; Zhang, Y.-Q.; Leng, X.-B.; Yang, M.-W.; Jiang, S.-D.; Wang, Z.-X.; Ouyang, Z.-W.; Deng, L.; Wang, B.-W.; Gao, S. Two-Coordinate Co(II) Imido Complexes as Outstanding Single-Molecule Magnets. *J. Am. Chem. Soc.* **2017**, *139*, 373−380.
(36) Zadrozny, J. M.; Telser, J.; Long, J. R. Slow magnetic relaxation in the tetrahedral cobalt(II) complexes $[Co(EPh)_4]^{2-}$ (E = O, S, Se). *Polyhedron* **2013**, *64*, 209−217.
(37) Zadrozny, J. M.; Xiao, D. J.; Atanasov, M.; Long, G. J.; Grandjean, F.; Neese, F.; Long, J. R. Magnetic blocking in a linear iron(I) complex. *Nat. Chem.* **2013**, *5*, 577−581.
(38) Karunadasa, H. I.; Arquero, K. D.; Berben, L. A.; Long, J. R. Enhancing the Magnetic Anisotropy of Cyano-Ligated Chromium(II) and Chromium(III) Complexes via Heavy Halide Ligand Effects. *Inorg. Chem.* **2010**, *49*, 4738−4740.
(39) Peng, Y.; Mereacre, V.; Anson, C. E.; Zhang, Y.; Bodenstein, T.; Fink, K.; Powell, A. K. Field-Induced Co(II) Single-Ion Magnets with

DOI: 10.1021/acs.inorgchem.8b00160
Inorg. Chem. 2018, 57, 3371−3386

mer-Directing Ligands but Ambiguous Coordination Geometry. *Inorg. Chem.* **2017**, *56*, 6056−6066.
(40) Jurca, T.; Farghal, A.; Lin, P.-H.; Korobkov, I.; Murugesu, M.; Richeson, D. S. Single-Molecule Magnet Behavior with a Single Metal Center Enhanced through Peripheral Ligand Modifications. *J. Am. Chem. Soc.* **2011**, *133*, 15814−15817.
(41) Zhang, Y.-Z.; Gomez-Coca, S.; Brown, A. J.; Saber, M. R.; Zhang, X.; Dunbar, K. R. Trigonal antiprismatic Co(ii) single molecule magnets with large uniaxial anisotropies: importance of Raman and tunneling mechanisms. *Chem. Sci.* **2016**, *7*, 6519−6527.
(42) Marriott, K. E. R.; Bhaskaran, L.; Wilson, C.; Medarde, M.; Ochsenbein, S. T.; Hill, S.; Murrie, M. Pushing the limits of magnetic anisotropy in trigonal bipyramidal Ni(II). *Chem. Sci.* **2015**, *6*, 6823−6828.
(43) Chen, L.; Wang, J.; Wei, J.-M.; Wernsdorfer, W.; Chen, X.-T.; Zhang, Y.-Q.; Song, Y.; Xue, Z.-L. Slow Magnetic Relaxation in a Mononuclear Eight-Coordinate Cobalt(II) Complex. *J. Am. Chem. Soc.* **2014**, *136*, 12213−12216.
(44) Drahos, B.; Herchel, R.; Travnicek, Z. Impact of Halogenido Coligands on Magnetic Anisotropy in Seven-Coordinate Co(II) Complexes. *Inorg. Chem.* **2017**, *56*, 5076−5088.
(45) Zhu, Y.-Y.; Zhang, Y.-Q.; Yin, T.-T.; Gao, C.; Wang, B.-W.; Gao, S. A Family of $Co^{II}Co^{III}_3$ Single-Ion Magnets with Zero-Field Slow Magnetic Relaxation: Fine Tuning of Energy Barrier by Remote Substituent and Counter Cation. *Inorg. Chem.* **2015**, *54*, 5475−5486.
(46) Bruno, R.; Vallejo, J.; Marino, N.; De Munno, G.; Krzystek, J.; Cano, J.; Pardo, E.; Armentano, D. Cytosine Nucleobase Ligand: A Suitable Choice for Modulating Magnetic Anisotropy in Tetrahedrally Coordinated Mononuclear Co^{II} Compounds. *Inorg. Chem.* **2017**, *56*, 1857−1864.
(47) Saber, M. R.; Dunbar, K. R. Ligands effects on the magnetic anisotropy of tetrahedral cobalt complexes. *Chem. Commun.* **2014**, *50*, 12266−12269.
(48) Sheldrick, G. M. A short history of SHELX. *Acta Crystallogr., Sect. A: Found. Crystallogr.* **2008**, *64*, 112−122.
(49) Stoll, S.; Schweiger, A. EasySpin, a comprehensive software package for spectral simulation and analysis in EPR. *J. Magn. Reson.* **2006**, *178*, 42−55.
(50) Neese, F. The ORCA program system. *Wiley Interdiscip. Rev. Comput. Mol. Sci.* **2012**, *2*, 73−78.
(51) Neese, F.; Petrenko, T.; Ganyushin, D.; Olbrich, G. Advanced aspects of ab initio theoretical optical spectroscopy of transition metal complexes: Multiplets, spin-orbit coupling and resonance Raman intensities. *Coord. Chem. Rev.* **2007**, *251*, 288−327.
(52) Van Lenthe, E.; van der Avoird, A.; Wormer, P. E. S. Density functional calculations of molecular hyperfine interactions in the zero order regular approximation for relativistic effects. *J. Chem. Phys.* **1998**, *108*, 4783−4796.
(53) Van Lenthe, E.; Baerends, E. J.; Snijders, J. G. Relativistic regular two-component Hamiltonians. *J. Chem. Phys.* **1993**, *99*, 4597−610.
(54) Weigend, F.; Ahlrichs, R. Balanced basis sets of split valence, triple zeta valence and quadruple zeta valence quality for H to Rn: Design and assessment of accuracy. *Phys. Chem. Chem. Phys.* **2005**, *7*, 3297−3305.
(55) Schaefer, A.; Horn, H.; Ahlrichs, R. Fully optimized contracted Gaussian basis sets for atoms lithium to krypton. *J. Chem. Phys.* **1992**, *97*, 2571−7.
(56) Smolko, L.; Cernak, J.; Dusek, M.; Miklovic, J.; Titis, J.; Boca, R. Three tetracoordinate Co(II) complexes $[Co(biq)X_2]$ (X = Cl, Br, I) with easy-plane magnetic anisotropy as field-induced single-molecule magnets. *Dalton Trans.* **2015**, *44*, 17565−17571.
(57) Zabrodsky, H.; Peleg, S.; Avnir, D. Continuous symmetry measures. *J. Am. Chem. Soc.* **1992**, *114*, 7843−7851.
(58) Chilton, N. F.; Anderson, R. P.; Turner, L. D.; Soncini, A.; Murray, K. S. PHI: A powerful new program for the analysis of anisotropic monomeric and exchange-coupled polynuclear d- and f-block complexes. *J. Comput. Chem.* **2013**, *34*, 1164−1175.
(59) Smolko, L.; Cernak, J.; Dusek, M.; Titis, J.; Boca, R. Tetracoordinate Co(II) complexes containing bathocuproine and single molecule magnetism. *New J. Chem.* **2016**, *40*, 6593−6598.
(60) Figgis, B. N.; Gerloch, M.; Mason, R. *Proc. R. Soc. London, Ser. A* **1964**, *279*, 210−228.
(61) Krzystek, J.; Park, J.-H.; Meisel, M. W.; Hitchman, M. A.; Stratemeier, H.; Brunel, L.-C.; Telser, J. EPR Spectra from "EPR-Silent" Species: High-Frequency and High-Field EPR Spectroscopy of Pseudotetrahedral Complexes of Nickel(II). *Inorg. Chem.* **2002**, *41*, 4478−4487.
(62) Cucos, P.; Tuna, F.; Sorace, L.; Matei, I.; Maxim, C.; Shova, S.; Gheorghe, R.; Caneschi, A.; Hillebrand, M.; Andruh, M. Magnetic and Luminescent Binuclear Double-Stranded Helicates. *Inorg. Chem.* **2014**, *53*, 7738−7747.
(63) Maganas, D.; Milikisyants, S.; Rijnbeek, J. M. A.; Sottini, S.; Levesanos, N.; Kyritsis, P.; Groenen, E. J. J. A Multifrequency High-Field Electron Paramagnetic Resonance Study of CoIIS4 Coordination. *Inorg. Chem.* **2010**, *49*, 595−605.
(64) Pilbrow, J. R. Effective g values for S = 3/2 and S = 5/2. *J. Magn. Reson.* **1978**, *31*, 479−90.
(65) Banci, L.; Bencini, A.; Benelli, C.; Gatteschi, D.; Zanchini, C. Spectral-structural correlations in high-spin cobalt(II) complexes. *Struct. Bonding (Berlin)* **1982**, *52*, 37−86.
(66) Novikov, V. V.; Pavlov, A. A.; Nelyubina, Y. V.; Boulon, M.-E.; Varzatskii, O. A.; Voloshin, Y. Z.; Winpenny, R. E. P. A Trigonal Prismatic Mononuclear Cobalt(II) Complex Showing Single-Molecule Magnet Behavior. *J. Am. Chem. Soc.* **2015**, *137*, 9792−9795.
(67) Shrivastava, K. N. Theory of Spin−Lattice Relaxation. *Phys. Status Solidi B* **1983**, *117*, 437.
(68) Singh, A.; Shrivastava, K. N. Optical-acoustic two-phonon relaxation in spin systems. *Phys. Status Solidi B* **1979**, *95*, 273.
(69) Liddle, S. T.; van Slageren, J. Improving f-element single molecule magnets. *Chem. Soc. Rev.* **2015**, *44*, 6655−6669.
(70) Maurice, R.; Bastardis, R.; Graaf, C. d.; Suaud, N.; Mallah, T.; Guihéry, N. Universal Theoretical Approach to Extract Anisotropic Spin Hamiltonians. *J. Chem. Theory Comput.* **2009**, *5*, 2977−2984.
(71) Rechkemmer, Y.; Breitgoff, F. D.; van der Meer, M.; Atanasov, M.; Hakl, M.; Orlita, M.; Neugebauer, P.; Neese, F.; Sarkar, B.; van Slageren, J. A four-coordinate cobalt(II) single-ion magnet with coercivity and a very high energy barrier. *Nat. Commun.* **2016**, *7*, 10467.
(72) Maganas, D.; Sottini, S.; Kyritsis, P.; Groenen, E. J. J.; Neese, F. Theoretical Analysis of the Spin Hamiltonian Parameters in $Co(II)S_4$ Complexes, Using Density Functional Theory and Correlated ab initio Methods. *Inorg. Chem.* **2011**, *50*, 8741−8754.

DOI: 10.1021/acs.inorgchem.8b00160
Inorg. Chem. 2018, 57, 3371−3386